Mission and System Design for In-Situ Resource Utilization in the Outer Solar System using Nuclear Propulsion Technologies

By

Julia Witham

B.S. Nuclear Engineering
Rensselaer Polytechnic Institute, 2020

Submitted to the Department of Nuclear Science and Engineering
in partial fulfillment of the requirements for the degree of

MASTER OF SCIENCE IN
NUCLEAR SCIENCE AND ENGINEERING

at the

MASSACHUSETTS INSTITUTE OF TECHNOLOGY

June 2023

Authored By: Julia Witham
                   Department of Nuclear Science and Engineering
                   May 17, 2023

Certified by: Koroush Shirvan
                   John C. Hardwick Associate Professor of
                   Nuclear Science and Engineering
                   Thesis Supervisor

Accepted by: Ju Li
                   Department of Nuclear Science and Engineering
                   Chair, Department Committee on Graduate Students

Mission and System Design for In-Situ Resource Utilization in the Outer Solar System using Nuclear Propulsion Technologies

by

Julia Witham

Submitted to the Department of Nuclear Science and Engineering
May 17, 2023, in partial fulfillment of the requirements for the degree of
Master of Science in Nuclear Science and Engineering

Abstract

The parameter space of a theoretical in-situ propellant acquisition system is examined for a sample return mission from trans-Neptunian destinations (>40au) using two theoretical spacecraft designs, which compare nuclear propulsion systems for impulsive and continuous thrust. Each available propellant substance is compared in each propulsion system. Propellant acquisition systems are shown to be less advantageous overall for continuous thrust missions, where the system mass must remain well below the roughly 6 tons of additional propellant otherwise necessary to affect the return journey in 5 years.

While the spacecraft using impulsive thrust could return in 50 years with roughly equal propellant mass in a Hohmann maneuver, it required more than 70 tons of additional hydrogen propellant at launch to be capable of a comparable transit time to the electric spacecraft. For impulsive spacecraft, the optimal propellant mass for a return transit varies based on system and propellant characteristics. These optimal values are found for each scenario and each system. Even relatively inefficient (< 20 mL/kWh) acquisition systems were found to be constrained by propellant tank size. The low density of propellants such as liquid hydrogen had a pronounced impact on collection strategy and ultimate production capacity, such that propellant tank capacity became a valuable resource for a spacecraft.

Optimal parameters and collection goals for the propellant acquisition system are described for each potential destination, such that the mission time is minimized while making full use of the available propellant capacity. Among the available substances in the Kuiper belt, nitrogen propellants are the worst options in terms of mission time, propellant mass, and collection time requirements. Using raw methane as propellant instead of a source of hydrogen can offer significantly higher ΔV and lower total processing requirements in some scenarios. Hydrogen extraction from methane via pyrolysis presented the best overall performance for both propulsion systems.

Thesis Supervisor: Koroush Shirvan
Title: John C. Hardwick Associate Professor of Nuclear Science and Engineering

Acknowledgments

Table of Contents

List of Figures

List of Tables

Chapter 1

Introduction

Nuclear propulsion technology is a next-generation solution for exploring and colonizing the solar system. While missions to Mars and the asteroid belt are pushing the limits of modern propulsion systems, these limits are not yet fully characterized for nuclear propulsion systems. Despite the nearly limitless energy available from a nuclear reactor, the performance of the best propellants and structural materials may still be insufficient to realize complex missions to the outer solar system, such as a sample return from an icy trans-Neptunian object. Such a sample return mission is particularly challenging due to the complex logistics involved in rendezvous and return journeys. However, surface operations may provide an opportunity to replenish propellant or enhance electricity generation by rejecting waste heat into the surrounding environment. If propellant acquisition at a distant destination is sufficiently feasible, it may enable a wider variety of missions using near-term technology and eventually provide an efficient means to develop infrastructure throughout the solar system.

1.1 Objectives

The objective of this thesis is to characterize the most critical parameters of a theoretical propellant acquisition system and determine the mission structures, propulsion technologies, and propellant materials that are most effective to use in conjunction. To do this, later analysis will investigate the feasibility and potential benefits of using natural volatiles in nuclear propulsion systems during outer solar system missions, particularly those involving a rendezvous and return from trans-Neptunian objects. Such analysis also serves to illustrate the upper limits of performance for missions to the outer solar system.

9

1.2   Nuclear Propulsion Systems

Current space propulsion systems generally rely on chemical or solar energy to energize propellant to provide high and impulsive thrust or low and continuous thrust respectively. Due to the limitations of chemical and solar energy, these systems struggle with missions beyond the inner solar system, but the energy of a nuclear reactor is sufficient to enable either propulsion regime regardless of the mission's destination.

1.2.1 Solid Nuclear Thermal Propulsion (SNTP)

The most straightforward application of nuclear technology for space propulsion is a solid--fuel reactor using thermal energy to exhaust propellant. These systems were originally developed in the 1960s by the United States and Soviet Union, but despite promising performance, a full-scale system was never deployed in space[1]. A SNTP reactor closely resembles a traditional power reactor with long metallic fuel rods but operates at the highest possible temperature allowed by the structural materials to maximize specific impulse. Due to the thermal limits, the specific impulse of the rocket is mainly correlated with the structural materials' limits, and the propellant in use (where the best performance is achieved with hydrogen gas due to its low molecular weight). A unique feature of NTPs compared to chemical rockets is that the nuclear core has enough stored energy to operate at >10-100 times the needed capacity for any realistic scenario.[2] Because a SNTP system serves to heat and exhaust the propellant, then so long as a particular substance does not pose a corrosion risk, a SNTP system could theoretically utilize a variety of propellants.[3]
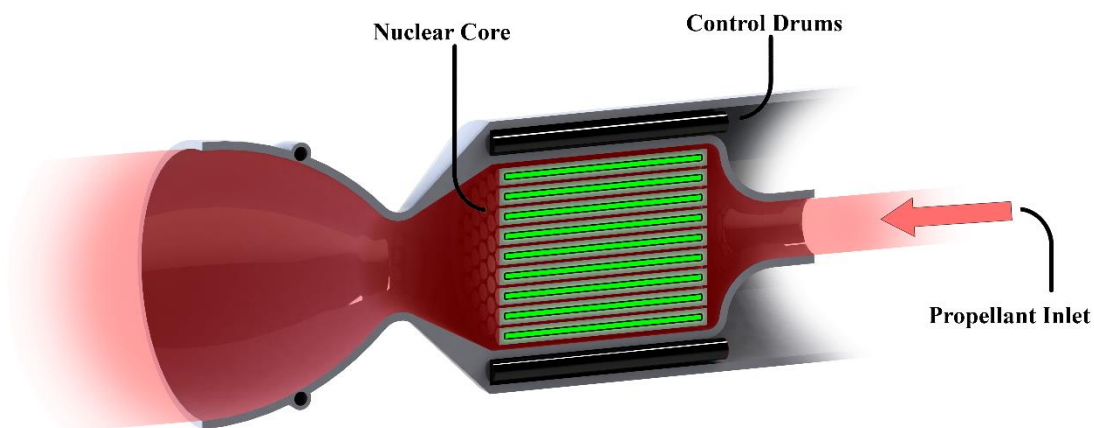
Figure 1: SNTP Core Cross Section

1.2.2 Centrifugal Nuclear Thermal Rocket (CNTR)

The Centrifugal Nuclear Thermal Rocket is a nuclear thermal propulsion concept intended to surpass the thermal limits on traditional SNTP systems.[4] By spinning the nuclear fuel elements at high speeds and allowing the nuclear fuel to melt inside them, each fuel element becomes a hollow channel or Centrifugal Fuel Element (CFE), which provides more direct heat transfer to the propellant. These centrifugal fuel elements have the additional advantage of maintaining contact with the coldest part of the fuel, while the hottest fuel "rises" toward the center of the channel. Propellant gas is "bubbled up" through the liquid fuel, which, at a temperature of 5500K, is hot enough to dissociate hydrogen gas for a maximum specific impulse of 1800s. This approach also provides an outlet for fission byproducts, many of which also exhaust alongside the propellant. Like an SNTP system, the CNTR could theoretically utilize various propellants, although some compounds like water still pose significant risk of corrosion. Research is ongoing to address these challenges and advance the CNTR towards practical application. Figure 2 shows the arrangement and function of CFEs inside a CNTR core.
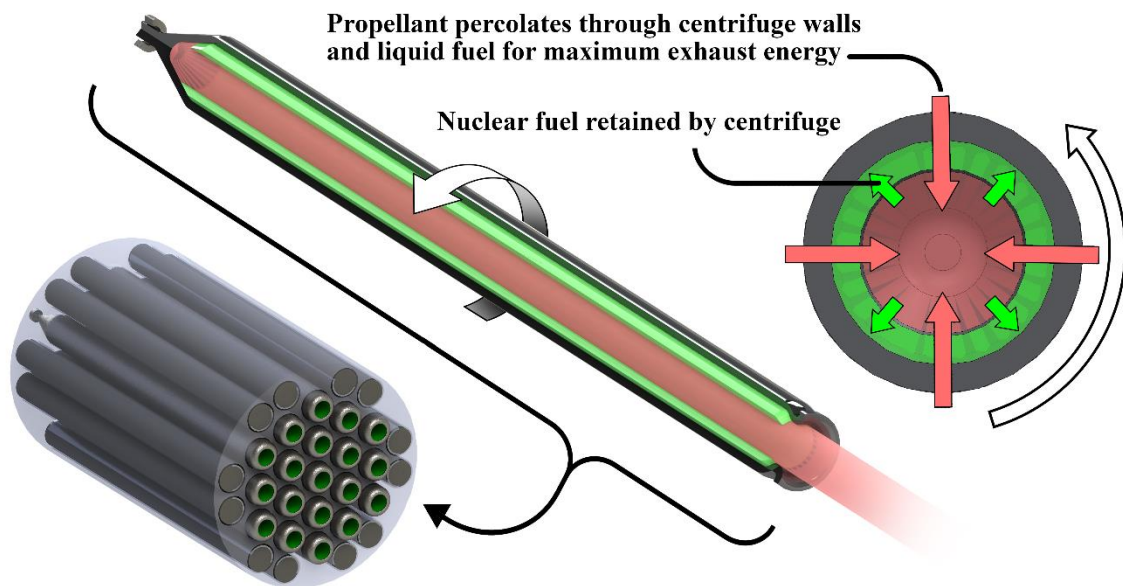
Figure 2: CNTR Fuel Element Arrangement and Function

For this study, the CNTR stands out as the best example of nuclear thermal propulsion to explore the feasibility of future high-performance missions. Throughout this thesis, the term NTP is used to refer to the nuclear thermal propulsion concept in general, but for the analysis section, all mentions of NTP refer to a system with CNTR performance, while any examples of SNTP are indicated explicitly.

1.2.3 Nuclear Electric Propulsion (NEP)

Nuclear electric propulsion systems use a nuclear powerplant to drive electric thrusters such as ion engines, Hall thrusters, or magnetoplasmadynamic (MPD) thrusters. NEP reactors do not interact with the propellant directly, and instead serve to drive on-board powerplants using a closed cycle powerplant and large radiators. Much like NTP, the power requirements of NEP barely scratch the surface of the available nuclear power, but these power systems work best with steep thermal gradients, which are only achievable using large radiators operating at very high temperatures, limiting maximum electrical power output. Even so, only the most powerful electric thrusters like MPDs can take advantage of these power levels (which can be kilowatts to megawatts depending on the payload). Even the most efficient MPDs run quite hot, with the best hydrogen-based prototypes[5] reaching only 50% efficiency, further squeezing the thermal budget of the radiator system.[6] Despite these challenges, this arrangement plays to the strengths of both the power and propulsion technologies, as both devices deliver optimal performance with a high and constant power for long periods of time. Nuclear electric propulsion systems offer a means of transporting large payloads efficiently, using long spiral trajectories that often covers a larger distance than the more direct path of an NTP system.

Traditional electric propulsion systems use heavier and more expensive propellants to maximize thrust and minimize mission time at smaller sizes. However, using larger amounts of lighter propellant with a bigger thruster is also a viable option, as hydrogen MPDs may approach[7] performance up to 8000 seconds. The latter strategy is essential to a spacecraft that recoups propellant at its destination, as heavy monatomic noble gasses are not readily available in the outer solar system.

1.3   In-Situ Resource Utilization (ISRU)

ISRU describes a wide range of technologies for producing propellant, water, oxygen, nutrients, and structural materials from natural resources in the space environment. During exploration, ISRU systems can provide additional propellant to extend a mission, such as NASA's concept to explore Triton with a nitrogen-collecting hopper spacecraft.[8] This thesis will examine the collection of raw volatiles for use as propellant, as well as additional chemical processing steps such as water electrolysis and methane pyrolysis. Both processes

are energy intensive methods of releasing hydrogen gas, but for nuclear spacecraft this energy investment may represent a worthwhile investment to improve mission capabilities. Figure 2 shows the design of an ISRU system for water ice powered by a nuclear reactor.

Figure 3: Nuclear Powered ISRU System for Hydrogen Extraction from Water Ice

For commerce and exploration throughout the solar system, volatiles (especially water) enable crewed or uncrewed missions to resupply propellant and efficiently extend missions. In a future where space travel is primarily nuclear (and thus limited more by propellant mass than by energy) ISRU systems would be essential to transform destinations with access to adequate materials into necessary waystations.[9] This analysis focuses on propellant acquisition from surface materials, with an emphasis on volatile ices in the outer solar system, however, the atmospheres of gas giants, comets, or the icy poles of planets like Mars all represent valuable supply caches to one day support the growth of commercial and industrial technology throughout the solar system.

1.4   The Kuiper belt and Kuiper belt objects (KBOs)

The Kuiper belt is a region of the outer solar system beyond Neptune that is home to several small, icy worlds known as Kuiper Belt Objects. Pluto, the most famous KBO, is a dwarf planet that was visited by NASA's New Horizons spacecraft in 2015.[10] Despite remote locations and small sizes, KBOs are of great scientific interest as they provide clues about the early history of the solar system and contain valuable resources such as water and other volatiles. However, exploring and studying KBOs is challenging due to their extreme distance from Earth and low surface gravity. These considerations indicate that advanced technologies will be essential for efficient exploration of KBO destinations.

Chapter 2

Kuiper Belt Exploration with ISRU

This section provides an overview of the destinations, propulsion systems, and mission architectures relevant to the analysis of Kuiper belt missions. Exploration beyond the orbit of Neptune offers a wide array of scientific and technological opportunities that are valuable for advancing our understanding of the universe and expanding space-exploration capabilities. To maximize the performance of a nuclear spacecraft exploring the Kuiper belt, an ISRU module could be used to collect and refine available materials. Several studies have considered scientific spacecraft with nuclear propulsion systems, and key examples are used as references for NTP and NEP missions. From these references, two comparable mission platforms were designed that reflect the stringent requirements of a theoretical sample return mission to the outer solar system. Each of these theoretical spacecraft require a unique mission architecture for the sample return objective, which accounted for the potential benefits of maneuvers like gravity assists, as well as the operation scheme of the reactor and ISRU systems.

2.1 Outer Solar System Destinations

Beyond Neptune, the rocky dwarf planets and asteroids of the Kuiper belt are too small to retain dense atmospheres. Among these trans-Neptunian objects, some are entirely barren and rocky, while others are composed entirely of water ice. All told, the KBOs present a wide range of sizes that effectively differentiate the available volatiles into unique combinations for each object. Among larger objects such as the dwarf planets Pluto and Eris, many different surface regions allow the concentrations of present compounds to vary significantly. The KBOs' average concentrations are shown in Table 1. Beyond Quaoar, the smaller KBOs can no longer retain volatiles, and are instead composed of heavier ices

like ammonia, water, and carbon dioxide. Ascertaining the exact percentages of these compounds is extremely difficult for such small objects, as even the rough ratio of rock to ice appears highly unpredictable.[11] The data in Table 1 was obtained through spectral analysis for all destinations besides Pluto.

Table 1: Surface compositions of KBOs

KBO	N$_2$	CH$_4$	H$_2$O	Average (%)
Pluto[10, 12]	>95%	<5%	x	
Eris[13]	30-70%	70-30%	0-10%	
Haumea[14]	x	x	>99%	
Makemake[11]	<10%	>90%	x	
Sedna[15]	<10%	<60%	<70%	
Quaoar[16]	2%	90%	7%	
Other KBOs[11]	x	x	>90%	

Based on these compositions, the Kuiper belt offers a limited number of potential propellant materials but does possess a sufficient range of object sizes and temperatures to stratify the available material. While some destinations possess a mixture of various ices, performance tradeoffs of mixed propellants will be discussed but not analyzed in depth. Analysis will focus on destinations like Pluto, Makemake, and Haumea, which are assumed to offer a single surface material only.

2.2 Available Propellant Materials and Key Destinations

Based on the range of surface compositions offered by the KBOs, the substances listed in Table 2 account for all viable propellant materials, with various challenges and utility. The specific heats are assumed to be constant for all temperatures, and the decomposition energy for methane corresponds to the release of 1 mol of H2 and not to full dissociation.

Table 2: Material Properties of Volatiles in the Kuiper Belt

Material	Molar Mass[17] (g/mol)	Decomposition energy ΔG[18] (kJ/mol)	Melting Point Liquid Density[17] (g/L)	Solid Density At 40K [19] (kg/m^3)	C$_p$[20] (300K) (kJ/kg*K)
Methane	16.04	37.7	422.8	525	2.25
Water	18.02	237	999.0	940	4.18
Nitrogen	28.01	933.5*	808.0	982	1.04
Hydrogen	2.02	431	70.9	N/A	10.2

---

* This is a back-of-the-envelope calculation using a dissociation energy of 9.675eV[21] and Avogadro's number

2.3 Outer Solar System Mission Platforms

Theoretical scientific missions to the outer solar system have previously been described for both nuclear thermal[22] and nuclear electric[23] propulsion-based spacecraft. The two-spacecraft presented in Figures 4 and 5 serve as key examples for missions of this scale.

Component	Mass (kg)
CNTP Engine	2,650
Propellant tanks	1,880
CNTP vehicle propellant	11,240
Spacecraft onboard propellant	900
Spacecraft bus and scientific payload	2,200
Total wet mass	18,880

Parameter	Case 1 (C3=0)
Power in the tug (kWe)	100
Mass of the tug (kg)	4000
Mass of the science payload (kg)	1000
Specific impulse (s)	10000
Efficiency of converting electrical to exhaust power (%)	75
Acceleration duration (yr)	3.79
Coast duration (yr)	7.00
Deceleration duration (yr)	2.24
Propellant mass used from C3=0 to KBO rendezvous (kg)	2984
Altitude of initial LEO (km)	N.A.
Isp for trip from LEO to C3=0 (s)	N.A.
Propellant mass from LEO to C3=0 (kg)	N.A.
Duration from LEO to C3=0 (yr)	N.A.
Total spacecraft wet mass at launch (kg)	7984
Total mission ΔV to rendezvous (km/s)	45.9
Total burn time to arrival (yr)	6.03
Total flight time to KBO rendezvous (yr)	13.03

Figure 4: NTP Spacecraft Characteristics
(Figure adapted from Ziehm and Thomas[21])

Figure 5: NEP Spacecraft Characteristics
(Figure reproduced from Houts et. al[20])

In both examples the scientific payload is expected to be approximately 1000kg, while the other support systems such as communications, navigation and spacecraft structure contribute another 1000kg. These assumptions offer a realistic starting point for later analysis using the ISRU system and comparing the propulsion techniques that use it. **Several modifications have been made to better compare these technologies and tailor them to a mission using ISRU:** The NTP concept (originally designed by Kumar et al.[24]) does not make explicit the electrical power conversion system necessary for scientific operation in the outer solar system, but a Brayton cycle generator is a fair assumption. Bimodal Nuclear Thermal Rocket (BNTR)[25] powerplants are designed to enable passive features, such as communications and life support, while an ISRU system is expected to be more energy intensive and require continuous operation for years during the mission[26]. These requirements make the ISRU system very similar to the nuclear electric propulsion systems, so assuming such a large powerplant (100 kWe) for both platforms will maximize the ISRU performance and enable direct comparison. This fortunately coincides with the operating range of minimally intrusive power sources (MIPS) under consideration for NTP concepts[27] as well as other next generation closed cycle generators[28]. For relevance to ISRU, the masses of the electric thruster and its power supply were recalculated for an MPD thruster using hydrogen plasma (1.25 kg/kW).[7] The original heatsink systems were assumed sufficient for continuous operation and considered part of the radiator system for mass calculations. Figure 6 and Table 3 show the arrangements and masses of each system.
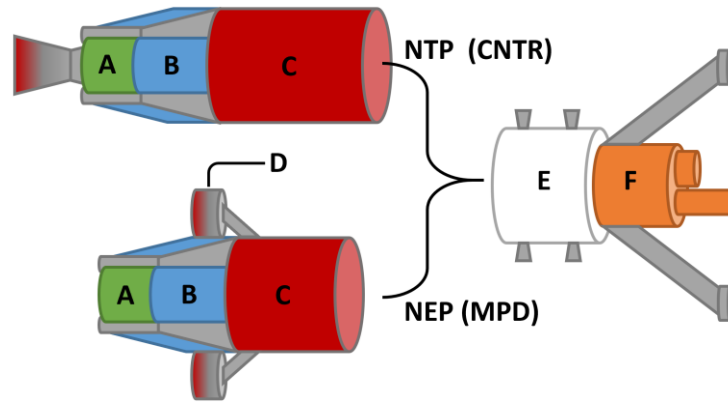
Figure 6: Spacecraft Systems

Table 3: Spacecraft Systems by Mass

Label	System	NTP Mass (kg)	NEP Mass (kg)
A	Nuclear Reactor & Shield	1,660	2,350
B	Powerplant & Radiators	940	
C	Original Propellant Tank	1,880	300
	Original H_2 Propellant Capacity	11,240	3,000
	New Propellant Tank	(See Figure 12)	
D	MPD Thruster and Power Supply	NA	500
E	Structure and Scientific Payload	2,000	
F	ISRU System	Varies	
	Total Dry mass Without ISRU or New Propellant Tanks	**4,600**	**4,850**
	Original Propellant Mass Fraction	(0.634)	(0.368)

2.4 Nuclear Propulsion System Characteristics

In Table 4, the features of the NEP and NTP systems used in this analysis are recorded for reference. A SNTP from NASA's Design Reference Architecture (DRA) 5.0 using a Bimodal Brayton powerplant has been provided for comparison.[25] Auxiliary propulsion systems were not considered in this analysis. SNTP and CNTR systems may not be capable of equal thrust, but this is not essential to later analysis assuming impulsive thrust.

Table 4: Nuclear Propulsion Systems

Power System	I_{sp} of H_2 (s)	Mass (kg)	Electrical Power	Full Power	Thrust	Mass Flow Rate per GW_{th}
NEP (MPD[7])	8000	2350	$100kW_e$	$333kW_{th}$	1.27N	0.048 kg/s
SNTP (BNTR[2])	1000	2224	$50kW_e$	$335MW_{th}$	66.7kN	20.3 kg/s
CNTR[29] (MIPS[27])	1800	1660	$100kW_e$	$335MW_{th}$	45kN	7.61 kg/s

2.5 ISRU Requirements and Parameters

The ISRU system for propellant acquisition and processing must:

- **Procure a sufficient mass of propellant material to replenish the spacecraft.**
- **Melt, pump, purify, store, and refrigerate propellant fluids after acquisition.**
- **Operate at a steady rate to maximize power utilization of the reactor.**
- **Remain well below the equivalent mass of propellant required without ISRU.**

These requirements translate to four key criteria that define the ISRU system in Table 5:

Table 5: Primary ISRU Parameters

ISRU Parameter	Units
Ultimate Production Capacity	kg
Ice Collection Efficiency	mL/kWh
Processing rate	kg/s
System mass	kg

2.6 General Mission Structure

To demonstrate the function of ISRU in this analysis, the spacecraft must not only intercept its first destination, but must also embark on a second trajectory. A return journey to earth is a reasonable conclusion for scientific missions, but final dispensation of the spacecraft on a KBO or multiple hops before return are also an option. The timeline of mission maneuvers and operations for a single destination and earth return are ordered in Figure 7, with NTP-specific maneuvers marked red, and NEP equivalents below each in green.
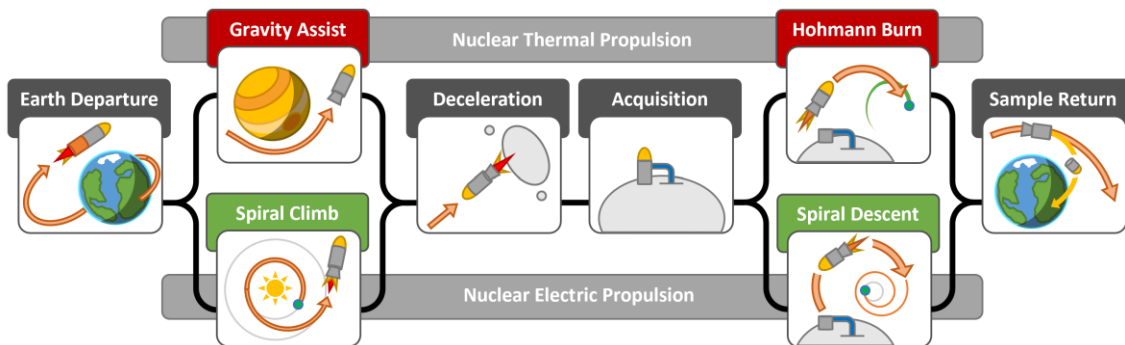
Figure 7: Mission Architecture for NTP and NEP

Earth departure can be achieved either with a C3 launch trajectory, or from a parking orbit, but for spacecraft of at least 10t with additional lift stages,[30] the main nuclear propulsion system will be necessary to begin an effective transit and to decelerate before KBO interception. Afterwards, the ISRU system will operate until sufficient propellant has been

collected for the next leg of the journey. If the ISRU is sufficiently heavy and easily detachable, it may also be possible to leave it behind before embarking on the final return trajectory for additional time savings. Finally, for the sample return, the entire spacecraft does not need to reenter
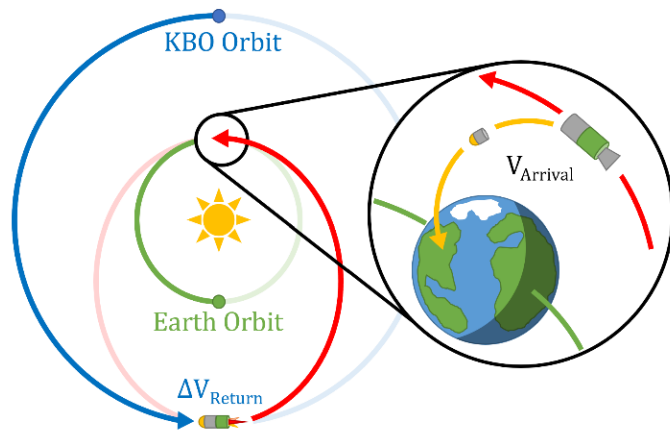
Figure 8: NTP Hohmann Return trajectory

earth orbit and can even depart the system once a payload has been dispatched towards the planet's surface. Several asteroid sample return missions have used this technique to reduce propellant requirements and transit times, including Hayabusa-2[31], which affected a successful sample return with a reentry velocity greater than 10km/s . Beyond the small requirements of a Hohmann burn, the return trajectory may also be sufficiently like a linear gravity freefall that an additional burn can be used to traverse the distance more quickly. This additional velocity must still be counteracted with a symmetrical burn before arrival to enable safe reentry, but if applicable, this technique may allow NTP to benefit from much larger quantities of propellant, and thus improve the proposition of ISRU.

2.7   Transit to and from KBO Destinations

Figure 9 illustrates the differences in propulsion scheme for NTP and NEP and notes the names of each maneuver as well as the relative thrust, duration, and format of the burns. In both cases, the analysis will focus on the return phase of each journey. **Due to the long-thrust periods and spiral trajectory optimal for electric acceleration and deceleration, gravity assist maneuvers do not offer NEP the same flexibility or additional ΔV compared to the near-impulsive burns of NTP.**
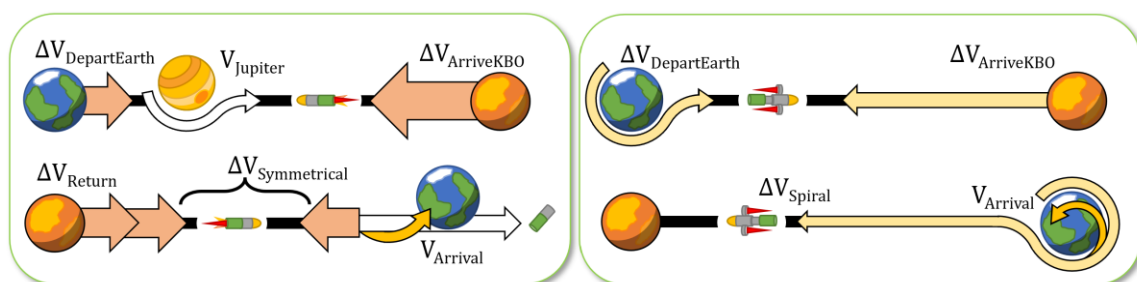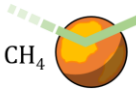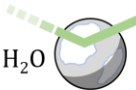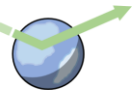
Figure 9: Propulsion Comparison for NTP (left) and NEP (right)

19

Once the initial transit is complete, propellant acquisition at the destination must be compatible with the propulsion device in use. Table 6 shows the rough performance of each surface concentration, although here note that not all materials are suitable for use as propellants, such as water, which poses substantial material challenges if used in its raw form. All of the destinations discussed here onward are viable for either propulsion technique, although more detailed analysis is required to assess the most appropriate propulsion system for each destination based on propellant performance. While most of these propellant and propulsion system combinations have been calculated previously, several are unique to this application. Using a simple formula for exhaust velocity, the performance of a CNTR using Nitrogen can be calculated using Equation 1 assuming molecular dissociation begins at approximately 3000K[21] and maintains a γ value of 1.36 at 5500K. The SNTP case does not assume dissociation as it operates closer to 3000K. For NEP, I_{sp} values come from literature[32].

$$I_{sp} = \frac{\sqrt{\frac{2 * \gamma_N}{\gamma_N - 1} * R * \frac{T_c}{m_N}}}{g} = 487.4 \ s \tag{1}$$

Table 6: Propulsion System Performance for each In-Situ Propellant Scenario (Values in parentheses are not chemically feasible)

KBO Surface Compositions	CH_4	H_2O	N_2
I_{sp} SNTP (s)	CH4 : 375 H2 : 900	(H2O : 314) H2 : 900	254 s
I_{sp} CNTR (s)	CH4 : 1000 H2 : 1800	(H2O : 1000) H2 : 1800	487 s
I_{sp} NEP (s)	H2 : 8000	H2 : 8000	1000 s

Based on the available surface materials and the multiple options available for utilizing methane in the CNTR, there are four different **scenarios** for propellant utilization that will be examined in the following section, in order of their complexity

1. NEP and NTP both using raw **Nitrogen**
2. NEP and NTP both using **Hydrogen** extracted from Water ice
3. NEP and NTP both using **Hydrogen** extracted from Methane ice
4. NEP using **Hydrogen** extracted from methane ice and NTP using raw **Methane**

Chapter 3

Analysis

Using the mission platforms and structures described previously, the initial mission requirements and return journey can be examined throughout the ISRU system's parameter space. Here the impulsive and continuous thrust strategies require significantly different techniques to compute, but while the ideal cases may show a clear tradeoff between the systems, the realistic operating points of the ISRU may not be beneficial for all missions.

3.1   Delta-V Requirements and Propellant Capacity

Unlike previous missions to the Kuiper belt (all of which have been high speed flybys), Spacecraft using ISPA must effectively cancel out the velocity gained by departure and assist maneuvers with a large deceleration burn to enable rendezvous and surface operations. While such deceleration burns are not a common feature of trajectory optimization, lower arrival velocities are still preferable to increase the time a mission spends in the vicinity of its scientific interest. For trajectories using a gravity assist, the optimal mission opportunities to KBO targets balance transit time and arrival velocity such that the total ΔV necessary for an interception is equal to the ΔV requirement of the Jupiter connection, plus the velocity upon arrival to the Kuiper belt. Among various optimized trajectories calculated for KBO destinations[33], an average ΔV requirement to affect assist maneuvers was 7.88km/s, while the corresponding arrival velocity was 14.68km/s. Together these parameters suggest that **22.5km/s** is a reasonable estimate for a KBO interception at an average of 45AU after **14 years**. The optimized gravity-assist trajectories found in literature focus on the most prominent KBO targets, so in addition to these bodies, trajectories to several smaller KBOs were examined in simulation to validate this assumption. Figure 10 shows one such trajectory to the KBO Ixion.[34]
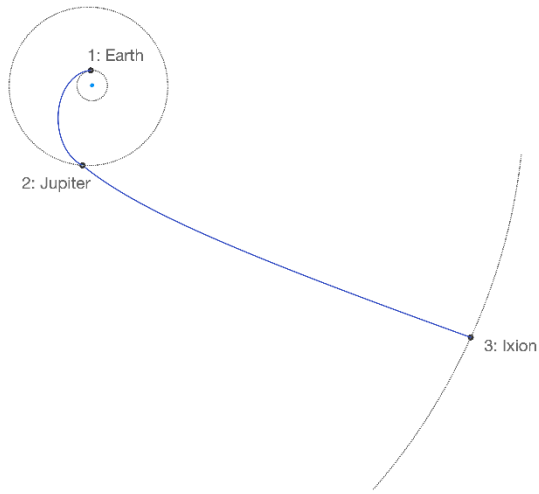
Figure 10: NTP Gravity Assist Trajectory to the Kuiper Belt
(Plotted trajectory provided courtesy of NASA JPL)

For NEP missions to the Kuiper belt, **53.4km/s** of ΔV is sufficient to depart earth and reach a KBO destination at 45AU in **13 years** using a spiral departure trajectory.[23] Figure 11 has been reproduced from Houts et. al. for comparison. Given the small variability between destinations, the transit time for both systems can be considered roughly equal.
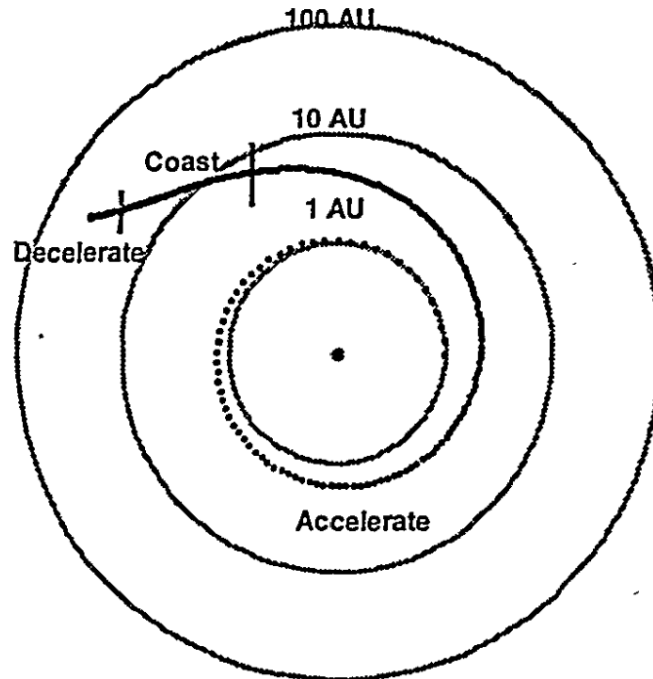
Figure 11: NEP Spital Trajectory to the Kuiper Belt
(Image reproduced from Houts et.al.[22])

Using the characteristics of the two mission platforms described in the previous section, and the mission requirements described above, the only remaining unknown when solving for the total propellant mass requirement is the mass of the ISRU system. Equation 2 shows the Tsiolkovsky rocket equation[35], and in this case the I_{sp} and ΔV requirements are fixed for each propulsion system, and after accounting for the mass of the propellant tanks, the resulting relationship between ISRU mass and spacecraft wet mass is almost linear. M represents a system, propellant, or spacecraft mass in tons. In this case ΔV is a fixed mission requirement given in m/s. The gravitational acceleration of the earth is given by g in m/s^2 and I_{sp} is the specific impulse in seconds.

$$M_{dry} = M_{wet} \exp\left(\frac{-\Delta V}{g * I_{sp}}\right) \tag{2}$$

$$M_{propellant}(M_{ISRU}) = (M_{ISRU} + M_{sc}) * \sqrt[(g*I_{sp})]{e}^{-\Delta V} - M_{ISRU} + M_{sc} \tag{3}$$

$$M_{tank}(M_{propellant}) = 0.1583 * M_{propellant}^{0.848} \tag{4}$$

Using the empirical formula[36] in Equation 4, the propellant mass requirement is used to find the mass of necessary propellant tanks, and the ultimate propellant requirements are found by iteration, the results of which are shown in Figures 12, 13, 14, and 15
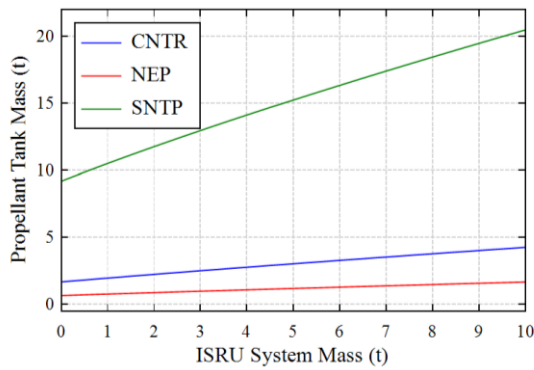
Figure 12: Propellant Tank Masses
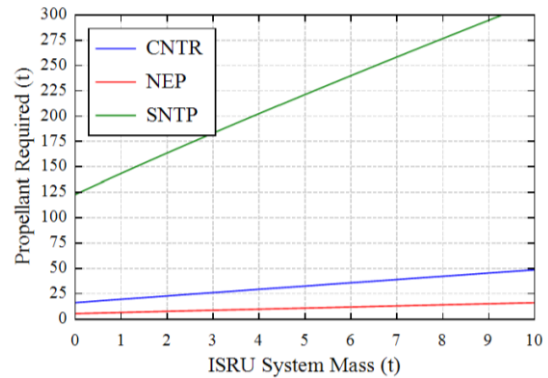
Figure 13: Propellant Requirements
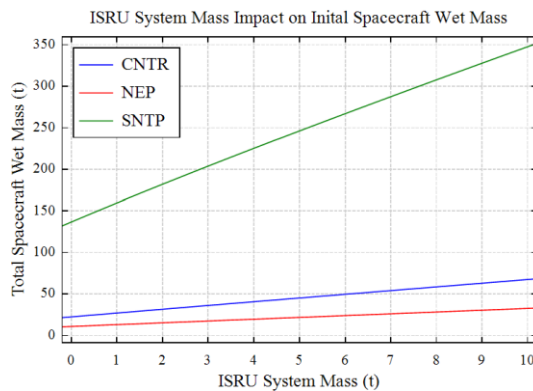
Figure 14: Wet Mass Comparison
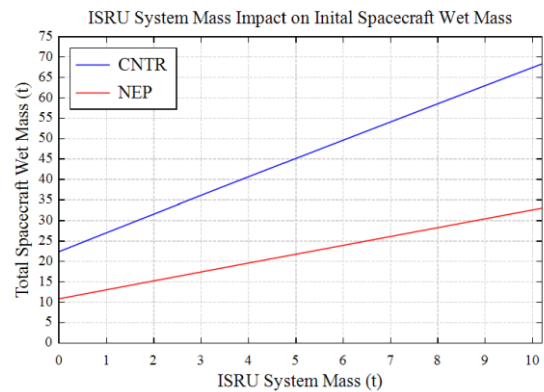
Figure 15: Wet Masses of NEP and NTP (This is a zoom-in of Figure 11)

23

3.2   Return Trajectories and Transit Times

Once surface operations on the KBO are complete, NEP and NTP will each require a different return trajectory to accommodate the fundamental differences between impulsive and continuous thrust. Gravity of the KBO is neglected for both maneuvers.

3.2.1   NTP return trajectory

For the high-thrust NTP, a Hohmann transfer is the most efficient means of returning to the lower orbit of earth. To pay for this efficiency, **the trajectory is extremely slow**, but due to the massive distances between earth and the KBOs, the time savings offered by traditionally **faster trajectories are ineffective** compared to their additional costs. The ΔV requirements and transfer time of Hohmann transfer between a KBO and earth are calculated are as follows, with variables illustrated in Figure 16, where V represents a velocity in m/s, R is a mean radius given in au, μ is the gravitational parameter of the sun with units m^3/s^2, and t is time (in this case found in years):

$$a = \frac{R_{Earth} + R_{KBO}}{2} \qquad (5)$$

$$V_{Earth} = \sqrt{\frac{\mu_{Sun}}{R_{Earth}}} \; ; V_{KBO} = \sqrt{\frac{\mu_{Sun}}{R_{KBO}}} \quad (6)$$

$$V_{Apoapse} = \sqrt{\mu_{Sun} * \left(\frac{2}{R_{KBO}} - \frac{1}{a}\right)} \qquad (7)$$

$$V_{Periapse} = \sqrt{\mu_{Sun} * \left(\frac{2}{R_{Earth}} - \frac{1}{a}\right)} \qquad (8)$$

$$\Delta V = V_{KBO} - V_{Apoapsis} \qquad (9)$$

$$t_{Transfer} = \pi \sqrt{\frac{a^3}{\mu_{Sun}}} \qquad (10)$$

$$V_{Arrival} = V_{Periapsis} - V_{Earth} \qquad (11)$$
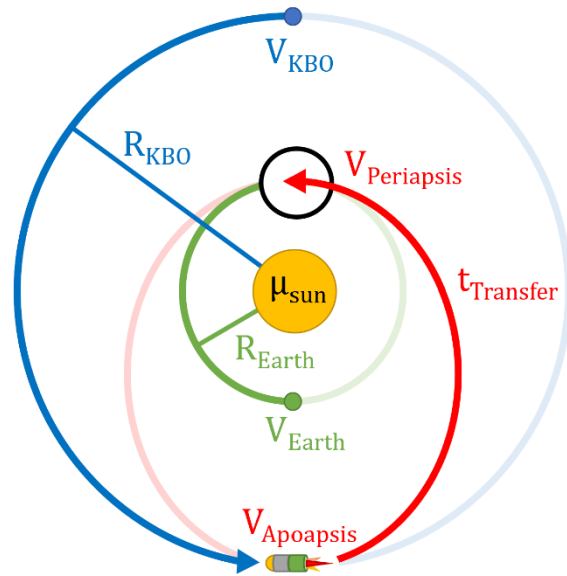
Figure 16: NTP Return Trajectory

Under normal circumstances a Hohmann transfer involves a second burn at arrival to circularize its orbit and match velocity with the target body, however this second burn is not strictly necessary for a sample return, as in the case of asteroid samples like Hyabusa-

2, which delivered samples via small re-entry modules[31]. This approach is also advantageous for a spacecraft using nuclear propulsion when reentry of the radioactive material is not an option. However, this approach must still account for the gravitational acceleration applied by the earth, or else risk reentry at an unacceptably high velocity. Equation 12 shows the balance of energy for this approach, where $V_{Reentry}$ represents the speed of the sample capsule entering the atmosphere, while $V_{Arrival}$ is the speed of the spacecraft, which will continue on its journey, both are given in m/s. G is the gravitational constant with units of $N*m^2/kg^2$, while M_E and r_E are the mass and radius of the Earth in tons and meters respectively. Table 7 lists the values of interest for transfers to earth from each of the selected KBO destinations based on their mean orbits[37].

$$\frac{G\ M_E\ M_{sc}}{r_E} + \frac{1}{2} M_{sc}\ V_{Reentry}{}^2 = \frac{1}{2} M_{sc}\ V_{Arrival}{}^2 \tag{12}$$

Under normal circumstances (like an Earth-Mars transfer), additional burns during a Hohmann maneuver would be counterproductive and inefficient. Here the extreme difference between the KBO orbit and earth's orbit result in a Hohmann maneuver that is essentially a **gravity freefall towards the sun.** This means that additional thrust and lower transit time can be achieved using equations for simple linear motion. Indeed, so long as the maneuvers are mirrored at either end of the journey (acceleration and deceleration) then ideally even the reentry velocities calculated previously will still be valid. Assuming equal acceleration and deceleration burns are performed with the leftover ΔV, then the total NTP transit time follows a $y = \frac{1}{x}$ trend based on the freefall time (Figure 17) and half of the leftover. In this way, **the Hohmann burn simply describes the requirements to enter the freefall phase of a return trajectory and approximate reentry velocity.**
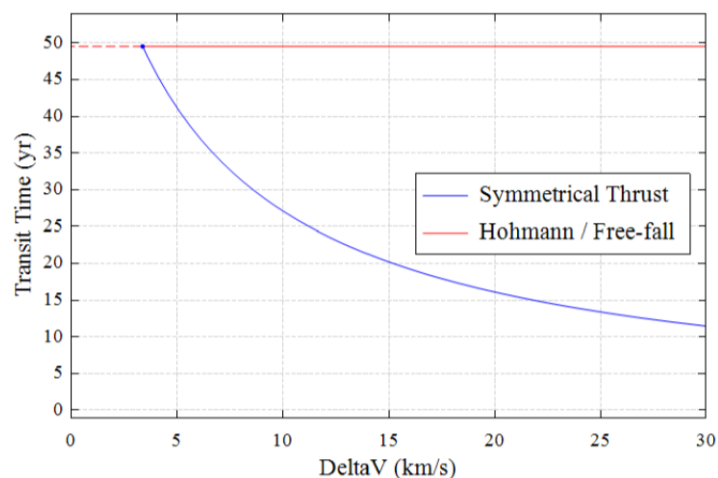
Figure 17: NTP Return Transit Time

Based on this curve, there is an intuitive tradeoff between propellant acquisition time and the transit afterwards. Depending on the parameters of the ISRU system, there will be an optimal balance between propellant acquisition time and the transit it enables. Figure 18 shows this calculation for one set of ISRU parameters (5t system mass and 25mL/kg acquisition using hydrogen from methane ice – values that will also be used to compare later examples), while the continuous optimal values are shown in detail in section 3.6.
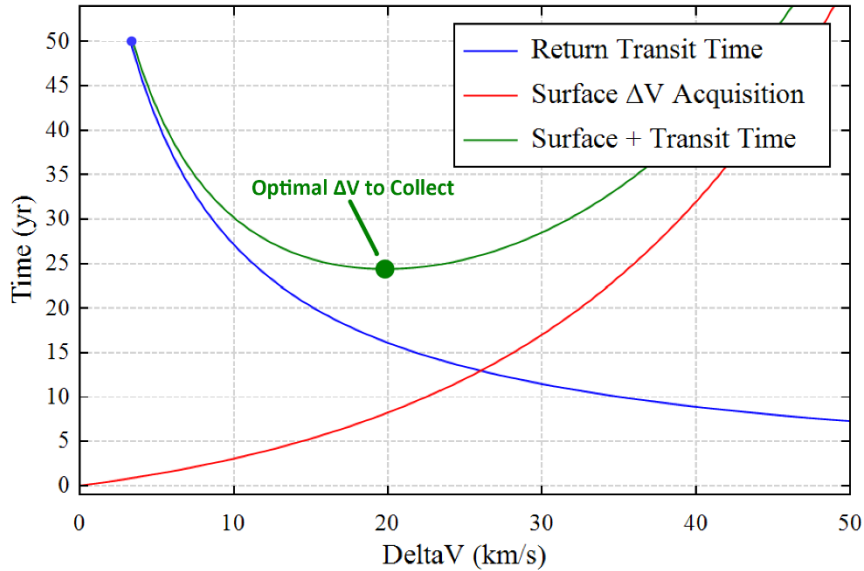
Figure 18: NTP Optimal Surface and Transit Time

3.2.2   NEP return trajectory

For the low-thrust NEP, the propulsion system must operate continuously in a spiral descent maneuver. The ΔV for such a maneuver can be roughly approximated as the difference between orbital velocities, as follows:

$$\Delta V_{spiral} = \sqrt{\frac{\mu_{Sun}}{R_{Earth}}} - \sqrt{\frac{\mu_{Sun}}{R_{KBO}}} \tag{13}$$

These values are present alongside the NTP mission parameters in Table 7, and the average will be used for future calculations in this analysis. Unlike NTP, the transit time of the continuous thrust maneuver will depend on both mass and thrust, as in the following formula for circle-to-circle maneuvers[38], where m is the average spacecraft mass:[39]

$$t_{spiral} = \frac{\Delta V}{F/m} \tag{14}$$

$$F_{MPD} = \frac{2 * P * \eta}{I_{sp} * g} = 1.274 \text{ N} \tag{15}$$

26

The thrust force for the MPD thrusters is calculated assuming an optimistic 50% efficiency and a constant specific impulse. It is important to note that Equations 13 and 14 are approximations, which are most accurate when the force of electric propulsion is much less than the force of the local solar gravity on the spacecraft. Figure 19 compares these forces as a function of distance throughout the solar system with planetary orbits for reference.
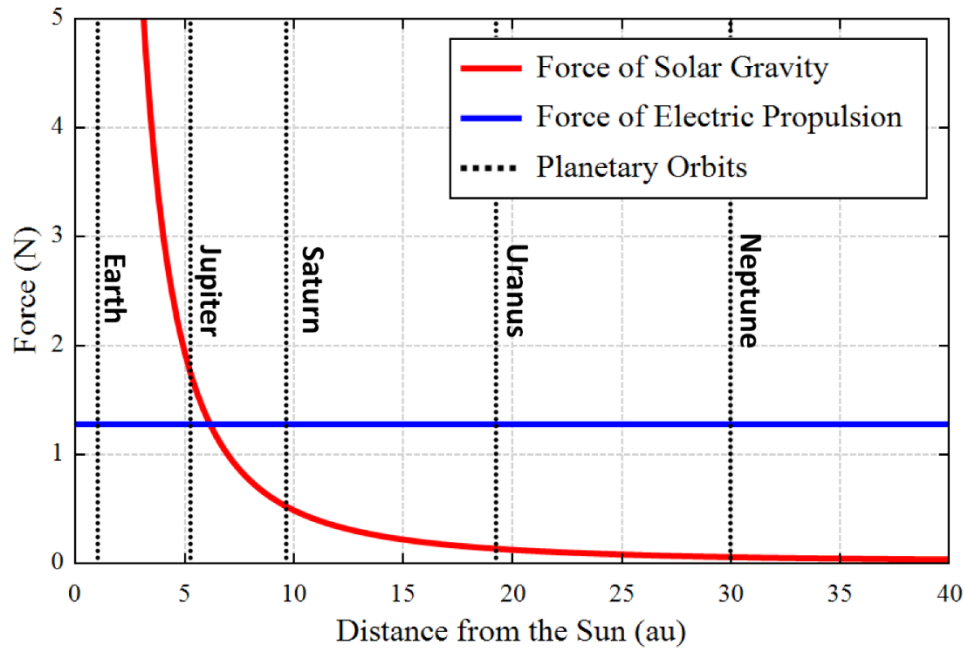
Figure 19: Forces of Solar Gravity and Continuous Thrust on the NEP Spacecraft

Based on the comparison in Figure 19, the assumptions used in later NEP calculations can be considered highly conservative for transit beyond Jupiter, as realistic transit would likely be even faster. This is partially the reason that the original outbound NEP trajectory required a deceleration burn to reach its KBO target. Despite this inaccuracy, these techniques are still sufficient to compare impulsive and continuous thrust mission architecture. Using these approximations, the transit time as a function of spacecraft mass is shown in Figure 20. The total mass involved includes the same propellant tanks as at the outset of the mission and compares their full capacity with a case where the tanks are only filled enough to satisfy the return maneuver's ΔV requirement and avoid carrying excess weight. Figure 20 also compares the transit times for a scenario in which the ISRU system is left on the KBO surface, in this case the propellant tanks are still differently sized depending on the original ISRU system mass at launch, but their impact is only barely noticeable and will not be discussed in further comparisons. Realistically, higher initial mass should also increase the initial transit time, but this will not be examined here.
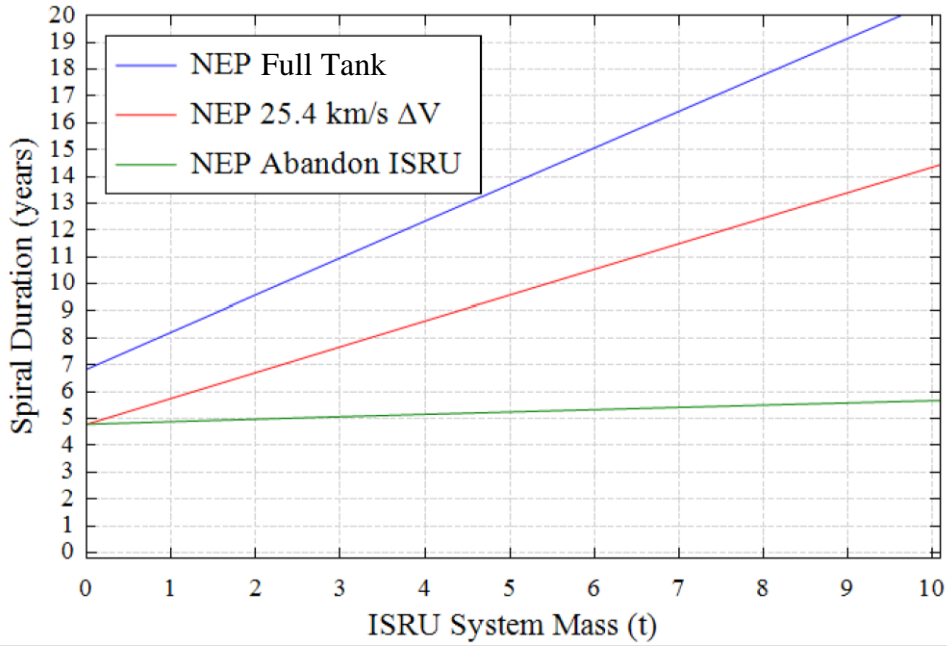
Figure 20: ISRU Mass impact on NEP return Transit

Key mission parameters are recorded in Table 7 for each of the propulsion systems and destinations. While each destination will require a unique mission structure, due to the extremely small variation between destinations, calculations using the parameters described are referenced according to the calculated averages to support general recommendations.

Table 7: Average Values of Key Mission Parameters

KBO	Mean Orbit (au)	NEP min Return ΔV (km/s)	NTP min Return ΔV (km/s)	NTP Hohmann Transfer Time (yr)	NTP $V_{Reentry}$ (km/s)
Pluto	39.48	25.04	3.69	45.5	14.92
Haumea	42.99	25.24	3.57	51.6	14.96
Makemake	45.34	25.36	3.50	55.7	14.98
Quaoar	43.7	25.28	3.55	52.8	14.96
Average	**42.88**	**25.23**	**3.58**	**51.4**	**14.96**

3.3   Energy Economics of Propellant Acquisition and Processing

Depending on the available surface ice composition and the propellant material required (e.g. whether pure methane is sufficient or if pure hydrogen is required) the processing times will be different. For the simplest case, where a surface material like raw methane or nitrogen will suffice as propellant, the rate of acquisition is intrinsic to the ISPA system.

28

In this case, the time spent on ISRU operations (as a function of ΔV desired) can be derived from the rocket equation by incorporating the reactor power, power conversion efficiency and ISRU performance: (Where R_{ISRU} describes the collection of KBO surface ice and is a constant with the units [kg/kWh]). For all cases, the conversion efficiency is assumed to be 30% for a Brayton cycle, and the peak thermal power is 334kW, which is a high but realistic idle power compared to other propulsion concepts.

$$t_{ISRU}(\Delta V) = \frac{m_{dry} * \left(-1 + \left(\sqrt[V]{e}\right)^{-\Delta V}\right)}{R_{ISRU} * \eta_E * Q_T} \qquad (16)$$

As in the case where water ice must be collected and decomposed to acquire hydrogen propellant, the addition of equipment such as an electrical device (e.g., electrolysis) adds a new load to the system, which lowers the overall acquisition rate. This electrolysis requirement is described by the new variable R_P for this "processing" step. Additionally, when the surface ice and propellant mass are not the same material, the molar ratio of those elements must also be included.

$$t_{ISRU}(\Delta V) = \frac{m_{dry} * \left(-1 + \left(\sqrt[V]{e}\right)^{-\Delta V}\right)}{\frac{\left(R_{ISRU} * \frac{m_{H2}}{m_{H2O}}\right) * R_P}{\left(R_{ISRU} * \frac{m_{H2}}{m_{H2O}}\right) + R_P} * \eta_E * Q_T} \qquad (17)$$

There are also situations where the propellant processing rate is driven by thermal energy instead of electrical energy (such as methane pyrolysis for hydrogen and carbon separation). In this case the processing rate takes advantage of the more abundant thermal power but must still compete with the power demands of the ISRU system.

$$t_{ISRU}(\Delta V) = \frac{m_{dry} * \left(-1 + \left(\sqrt[V]{e}\right)^{-\Delta V}\right)}{\frac{\left(R_{ISRU} * \frac{2 * m_{H2}}{m_{CH4}} * \eta_E\right) * R_P}{\left(R_{ISRU} * \frac{2 * m_{H2}}{m_{CH4}} * \eta_E\right) + R_P} * Q_T} \qquad (18)$$

Together, these three equations describe the ISRU operation for each of the key surface compositions relevant to the outer solar system. Depending on an ISRU system's actual approach (mining/drilling, melting/pumping, etc.) the ISRU Rate may be better described in terms of volume of surface ice per kilowatt hour, in which case the properties of the surface material at the appropriate temperature are required.

$$t_{ISRU}(\Delta V) = \cfrac{m_{dry} * \left(-1 + \left(\sqrt[V]{e}\right)^{-\Delta V}\right)}{\cfrac{\left(R_{ISRU}\left[\frac{cm^3}{kWh}\right] * \rho_{CH4} * \frac{2 * m_{H2}}{m_{CH4}} * \eta_E\right) * R_P}{\left(R_{ISRU}\left[\frac{cm^3}{kWh}\right] * \rho_{CH4} * \frac{2 * m_{H2}}{m_{CH4}} * \eta_E\right) + R_P} * Q_T} \tag{19}$$

The energy investment for the processing step is measured in kilograms of propellant material and varies depending on the surface ice being processed. This processing step is only present when the propellant material is not the same as the surface ice. For methane pyrolysis and water electrolysis the processing energy is calculated following equation 20.

$$R_{Pyrolysis} = \frac{m_{H_2}}{\Delta G_{CH_4}} = \frac{2.02 \frac{g}{mol}}{37.7 \frac{kJ}{mol}} = \boldsymbol{0.1929} \ \frac{kg}{kWh} \tag{20}$$

$$R_{Electrolysis} = \frac{m_{H_2}}{\Delta G_{H_2O}} = \frac{2.02 \frac{g}{mol}}{285.8 \frac{kJ}{mol}} = \boldsymbol{0.0254} \ \frac{kg}{kWh} \tag{21}$$

3.4   Propellant and Propulsion System Performance

Both NEP and NTP (e.g., CNTR) systems will perform differently based on the propellant used. Unlike Nitrogen, volatiles like water and methane also present the opportunity to extract and use pure hydrogen using additional machinery. While energy intensive, this does improve the ΔV available per kilogram of propellant, but substantially diminishes the overall propellant mass collection rate as described in Equation 18. Regardless of ISRU outcome, the performance of raw methane versus the processed hydrogen is compared for each propulsion technology in Figures 21, 22, and 23. For these comparisons, each spacecraft is assumed to have a weightless ISRU module for clarity. These calculations are directly derived from the Tsiolkovsky rocket equation (22), where for hydrogen extraction, the propellant mass is multiplied by the unitless mass fraction w_i of hydrogen compared to the surface ice. Methane is roughly 25% hydrogen by mass, whereas water is only 11.2% hydrogen by mass. Therefore, in the case where the raw substance of surface ice will suffice as propellant, the mass fraction of propellant to surface ice is effectively 1.

$$m_{dry} = m_{wet}e^{-\frac{\Delta V}{V_e}} \tag{22}$$

$$\Delta V(m_{ice}) = \ln\left(\frac{m_{ice} * m_i + m_{dry}}{m_{dry}}\right) * I_{sp} * g \tag{23}$$
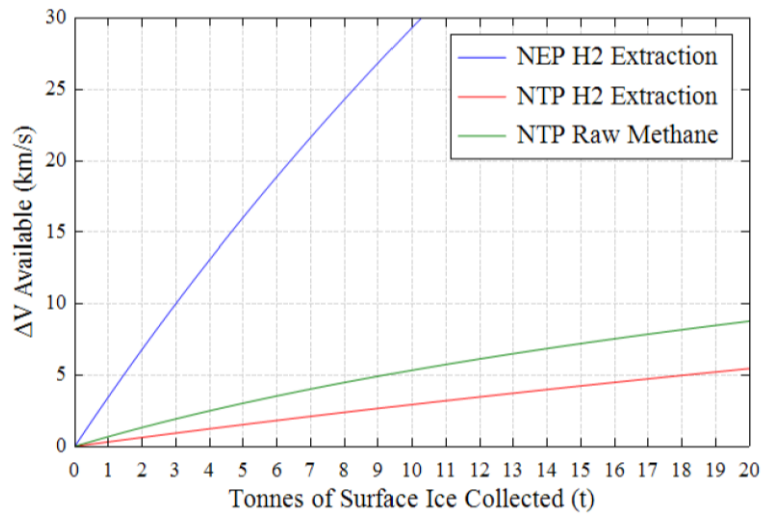
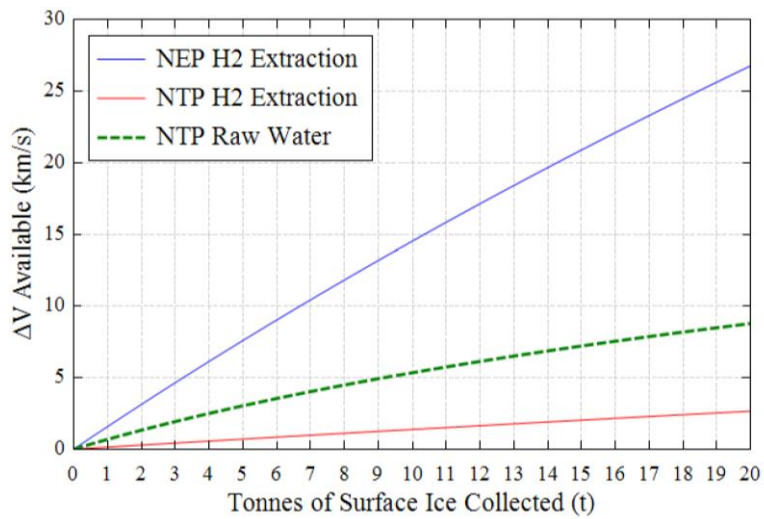**Figure 21: Utilization of Methane Ice**

Figure 22: Utilization of Water Ice
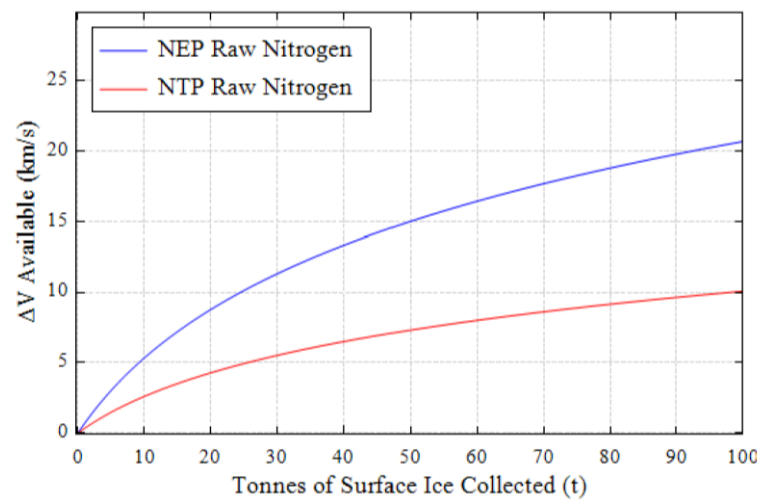(Dashed lines indicate infeasible chemistry)

Figure 23: Utilization of Nitrogen Ice

In Figure 22, the line indicating raw water propellant for the CNTR is dashed to indicate the chemical limitations on device operation, but it is still included for comparison. For both impulsive and low thrust systems, the use of heavier molecules is disadvantageous in terms of ΔV, even though the NEP system benefits from higher thrusts. The comparison between NEP and NTP for Nitrogen propellant is more dynamic than methane or water, as the diminishing returns are more evident when much more mass is necessary to reach the ΔV requirements. This relationship is illustrated in Figure 23. In this case a NEP system might realistically require another MPD thruster tailored to use Nitrogen efficiently or might have even set out from Earth with nitrogen propellant. However, while heavy molecules like nitrogen may provide additional thrust, the MPD efficiency can fall as low as 10% when operating in this regime[32]. Therefore, even if the thrust force is slightly higher, the additional energy requirement of the waste heat is assumed to balance out any such benefits from nitrogen propellant, such that none of these considerations shift ΔV directly.

3.5   ISPA System Performance for each Propellant Material

In the following sections, the ISRU systems are characterized based on collection efficiency and overall system mass. The collection efficiency is a theoretical metric that describes the volume of surface ice collected for one kilowatt hour of electrical input to the system. This includes the drilling, heating, pumping, and any other steps necessary to collect propellant, except for the free energy necessary to dissociate hydrogen-bearing molecules where applicable. The exact methods of surface ice collection are beyond the scope of this analysis, but in all cases, the solid surface ice will need to be melted to be compatible with the systems described thus far. In order for electrolysis to be feasible, the water must be liquid. As well for cases using methane pyrolysis, the material must also be heated to at least 1000ºC for the process to take place. In each case, the target temperature and minimum energy investment to reach it are displayed in Table 8. All these considerations help to define the thermodynamic maximum for the ISRU collection efficiency. For simplicity, these calculations assume a constant specific heat for each material and include the heat of fusion for the ice, and the enthalpy of vaporization[17] where appropriate, and assume processing at one atmosphere before propellant storage.

Table 8: Energy Requirements for Surface Ice Collection

Process	ΔT required for collection	Energy Investment (kWh / L)	100% Collection Efficiency (L / kWh)
Methane Collection	40 K → 111.6 K	0.032	31.3
Methane Pyrolysis	40 K → 1273 K	0.484	2.06
Water electrolysis	40 K → 273.2 K	0.342	2.93
Nitrogen Collection	40 K → 111.6 K	0.014	74.1

3.6   ISPA Operations for each Scenario

The impacts of various ISRU parameters are presented for each destination in the sections afterward. For efficient ISRU devices, the overall propellant capacity is one of the key limits on spacecraft performance. Depending on the mass of the ISRU system at launch, the capacity of the propellant tanks is assumed fixed, however if the ISRU is left behind thereafter, its tanks are oversized relative to the new mass and provide higher ΔV than at the outset of the mission. Such trends are shown below in Figures 24 and 25 for NTP and NEP, respectively. Entries marked with an * indicate that the ISRU was left behind.
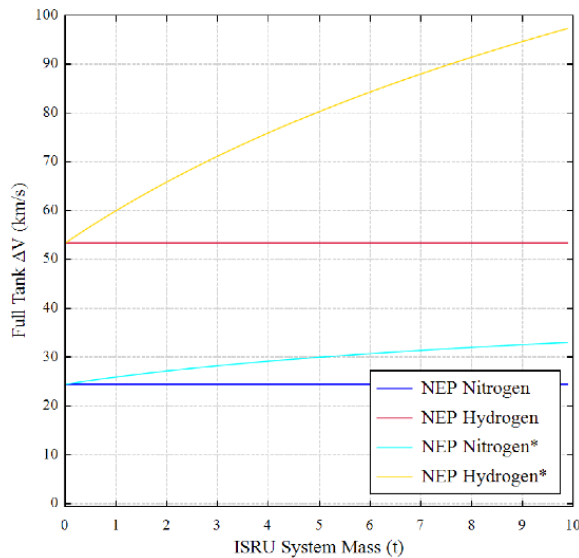
Figure 24: NTP Full Tank ΔV
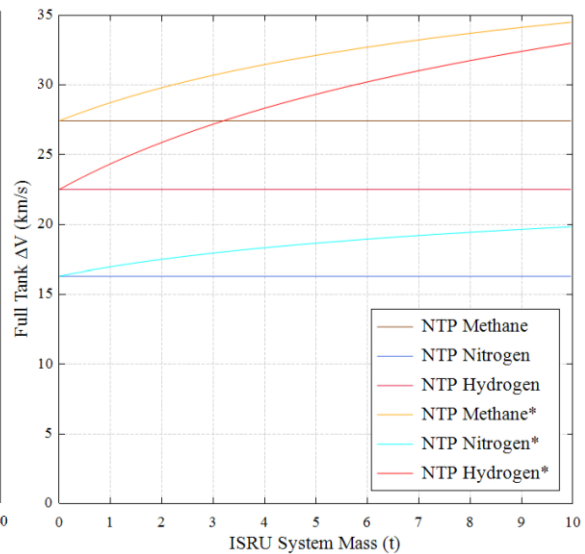
Figure 25: NEP Full Tank ΔV

The maximum ΔV capacities for each propellant are effectively constant for all cases where the ISRU system is retained, however, if the ISRU system is detached before the return journey, then a full propellant tank can offer higher ΔV to the spacecraft overall.
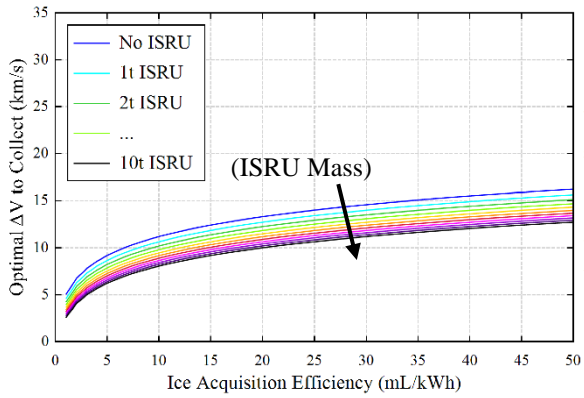
Figure 26: Optimal ΔV using Raw Nitrogen
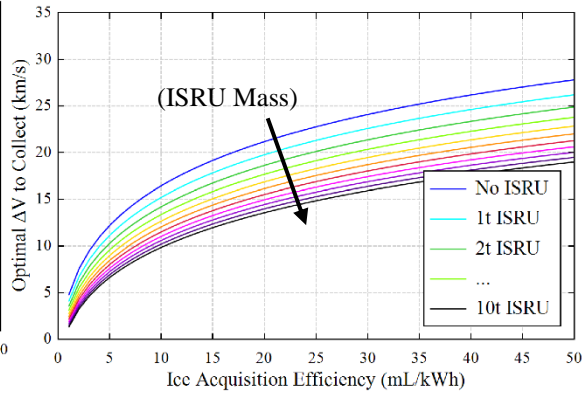
Figure 27: Optimal ΔV Using H_2 from H_2O
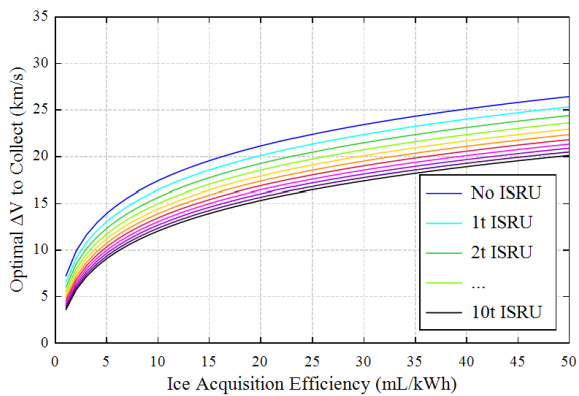
Figure 28: Optimal ΔV using Raw Methane
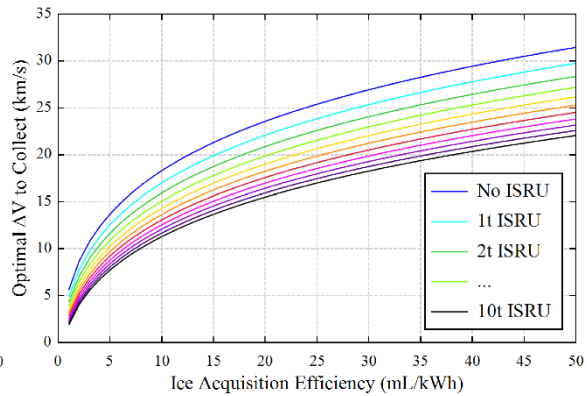
Figure 29: Optimal ΔV using H_2 from CH_4

Regardless of the spacecraft's actual propellant capacity, the ISRU system parameters and the surface composition of the KBO will determine the optimal amount of ΔV to collect to minimize the total surface plus transit time. This dynamic was described previously in Figure 18 and is calculated here in Figures 26, 27, 28, and 29 for each ISRU scenario. The corresponding surface times for each optimal collection period have been plotted alongside the equivalent NEP scenario in each of Figures 30 to 36. Compared to the other scenarios, the surface time for raw methane collection in NTP does not have a direct analog for the NEP regime, but despite the reduced complexity of this approach, the total collection time is very similar to the other cases.
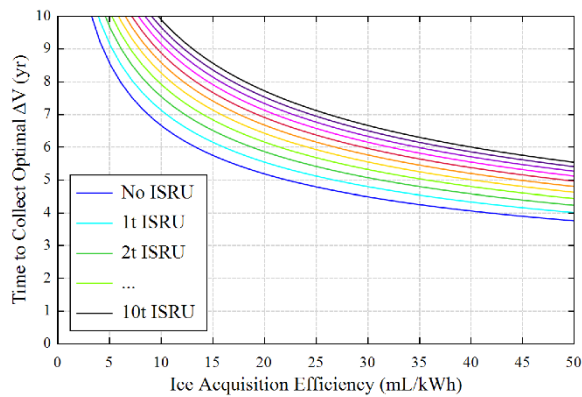
Figure 30: NTP using Raw Methane

34

3.6.1   Nitrogen-Rich Destinations
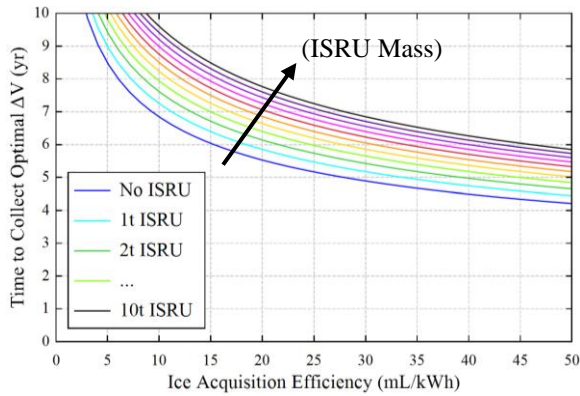
Figure 31: NTP using Raw Nitrogen
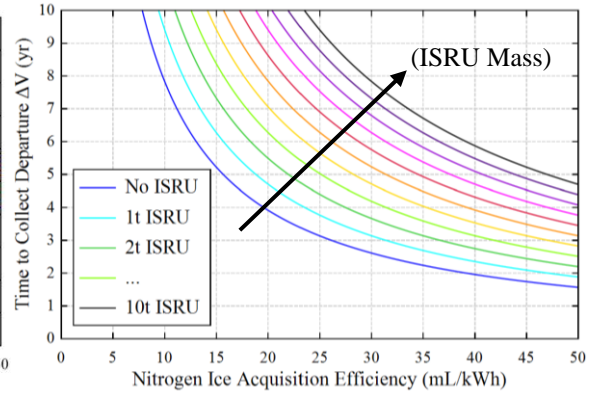
Figure 32: NEP using Raw Nitrogen

3.6.2   Water-Rich Destinations
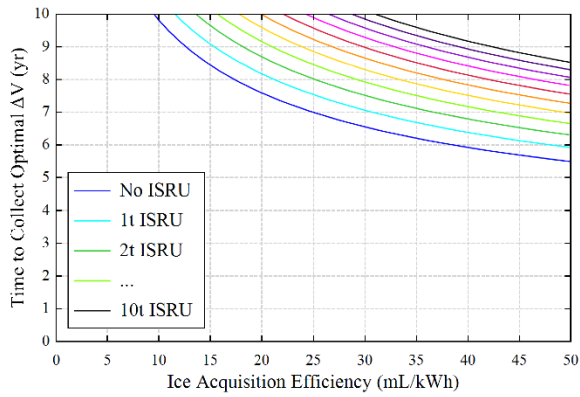
Figure 33: NTP using H$_2$ from H$_2$O
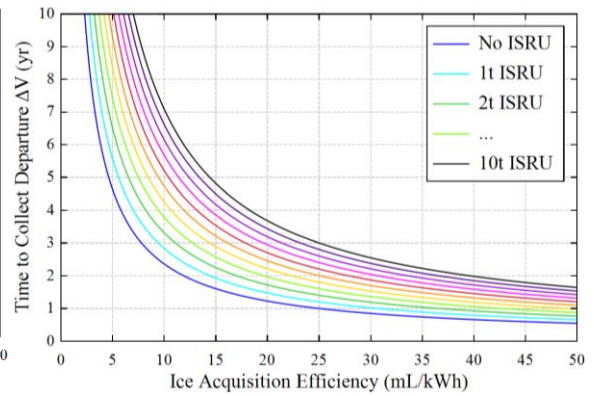
Figure 34: NEP using H$_2$ from H$_2$O

3.6.3   Methane-Rich Destinations
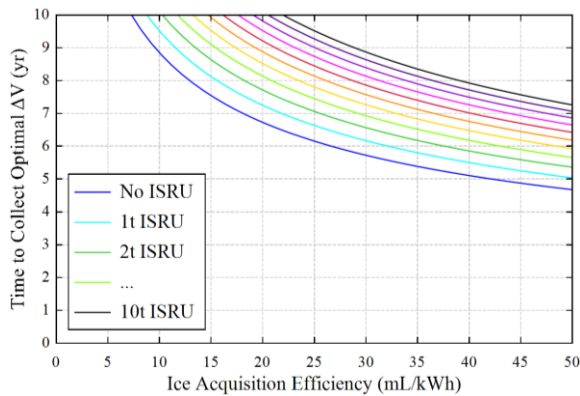
Figure 35: NTP using H$_2$ from CH$_4$
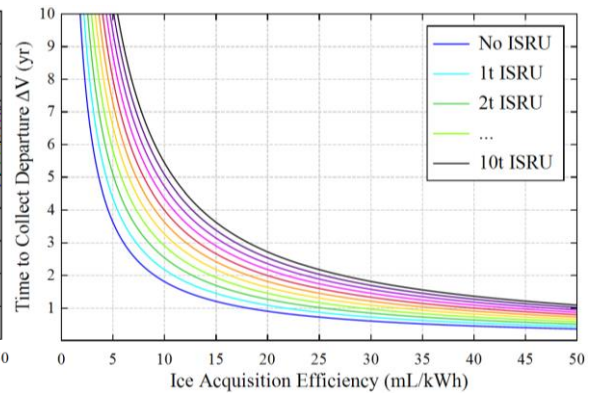
Figure 36: NEP using H$_2$ from CH$_4$

3.7 ISRU Impact on Ideal NTP Mission Time

Figures 37 through 40 illustrate the return transit times for NTP by adding together the surface and transit time calculated for each optimal ΔV. In each case, the transit time is almost always longer than the time spent acquiring propellant, but due to the related rates between these operations, the times spent on each phase were of the same order for all but the lowest efficiencies. For each calculation, any time spent in transition from surface operations to return transit was considered negligible, and surface operations were assumed to be uninterrupted regardless of collection period.
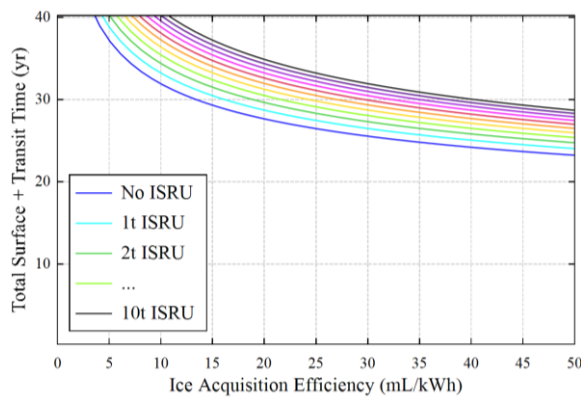
Figure 37: Mission Time using Raw Nitrogen
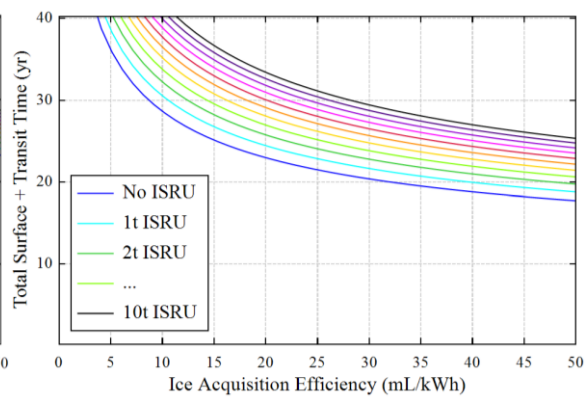
Figure 38: Mission Time using H_2 from H_2O
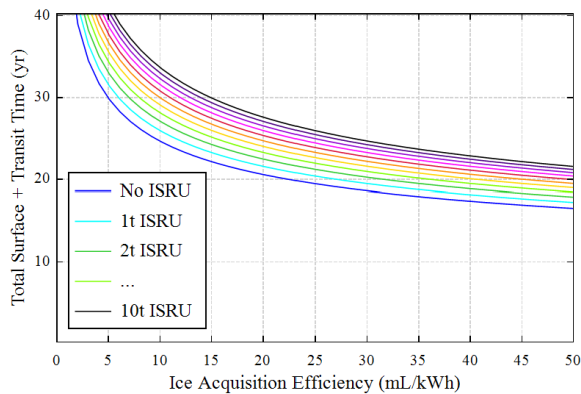
Figure 39: Mission Time using Raw Methane
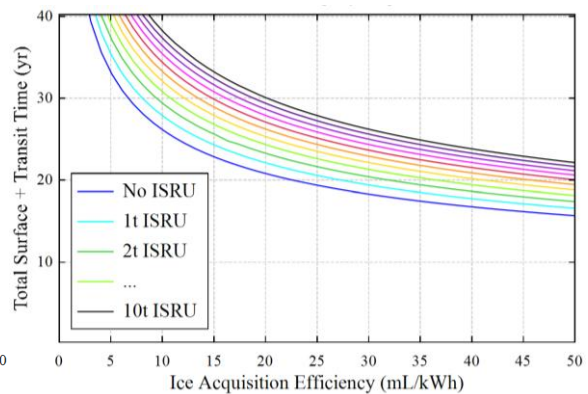
Figure 40: Mission Time using H_2 from CH_4

In each following subsection, these transit times are compared with the more linear return transit relationships for the NEP system. Where applicable, the results of this comparison indicate which technology demonstrates a lower mission time based on the ISRU parameters, and the destination surface composition.

3.7.1 Nitrogen-Rich Destinations
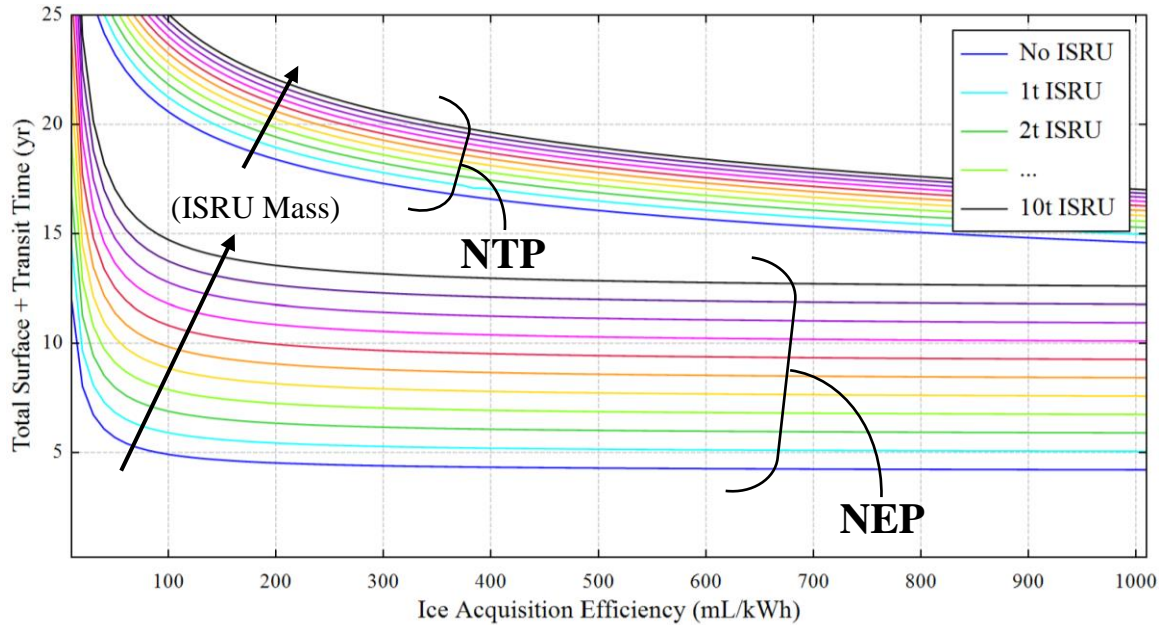
Figure 41: Mission Time Comparison for Raw Nitrogen

Figure 41 shows the trends in mass and efficiency dependence between NEP and NTP systems. For NEP with fixed ΔV requirements and constant thrust, a heavier ISRU system increases the propellant mass requirement and slows down the return transit. By contrast, NTP transit time does not explicitly depend on spacecraft mass and in this case can benefit from ΔV in excess of the minimum required to leave. This means that time spent on the surface collecting propellant can effectively subtract from the time in transit—**thus NTP systems are more sensitive to ISRU efficiency, while NEP systems are more sensitive to ISRU mass.** If the energy demands of operations like pumping and drilling are much larger than the thermal energy necessary to collect the material, there is no visible crossover between the performance of NTP and NEP within the range of realistic parameters. Figure 42 illustrates the overall ISRU efficiency where the maximum value corresponds to the maximum collection efficiency thermodynamically possible (noted previously in table 8). The following comparisons for the other propellants each examine a range of that corresponds to the thermodynamic requirements of the propellant material in question, where 100% efficiency indicates that the only energy requirements of the ISRU are the minimum necessary to heat the propellant, and 50% indicates that the pumping/drilling/refrigeration require an equal amount of energy per volume of propellant to the base thermal investment for collection.
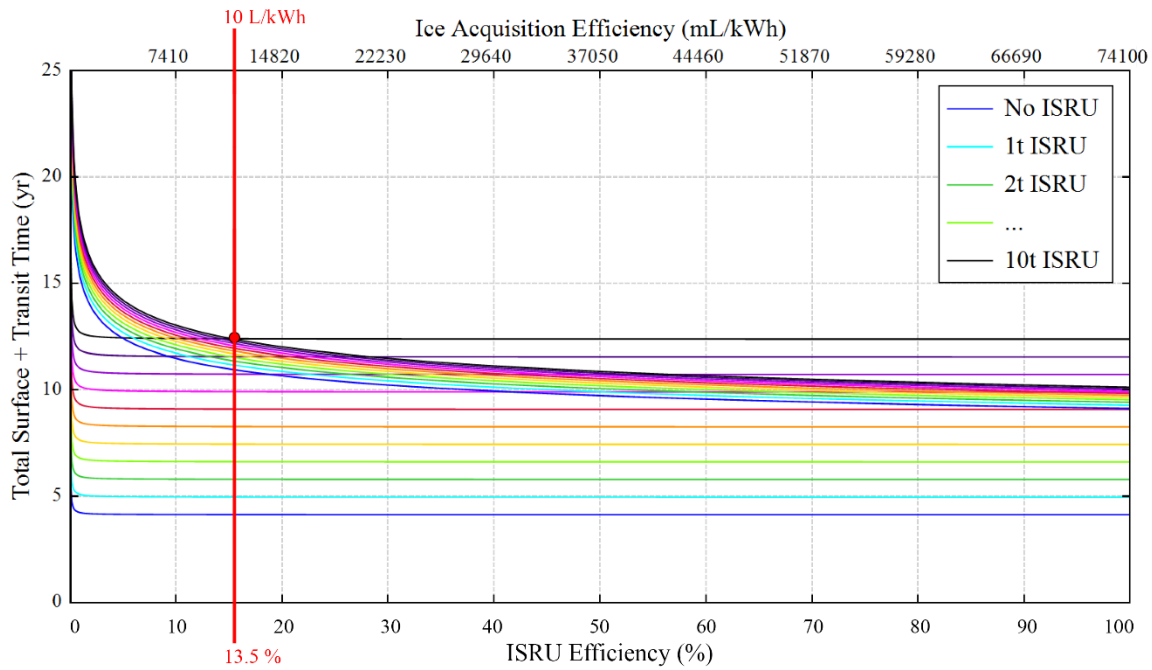
Figure 42: Ideal Mission Times using Raw Nitrogen

The relationship plotted in Figure 42 indicates that collecting surface ice at a rate of roughly 10 L/kWh (roughly 13% of the maximum theoretical efficiency) while using a 10t ISRU results in an equal mission time for both propulsion technologies. By plotting this relationship of equal mission time, Figure 43 shows where the noted propulsion technology provides superior return transit time across the range of ideal efficiency.
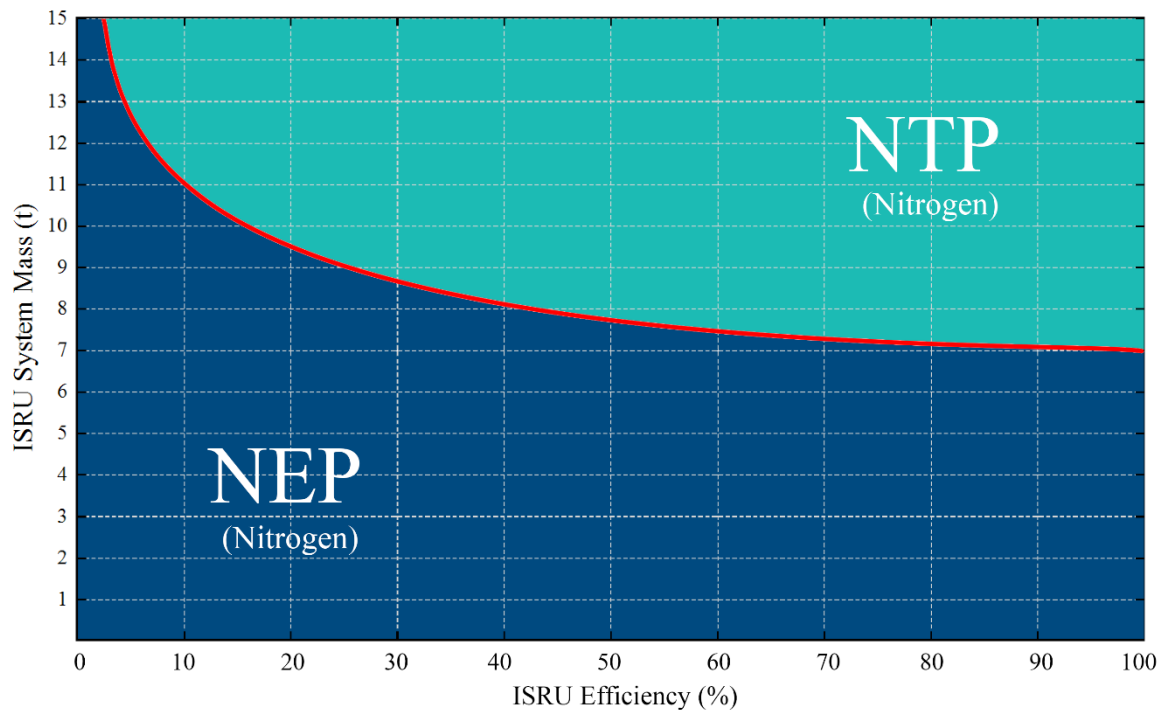
Figure 43: Ideal Propulsion using Nitrogen Propellant

3.7.2   Water-Rich Destinations
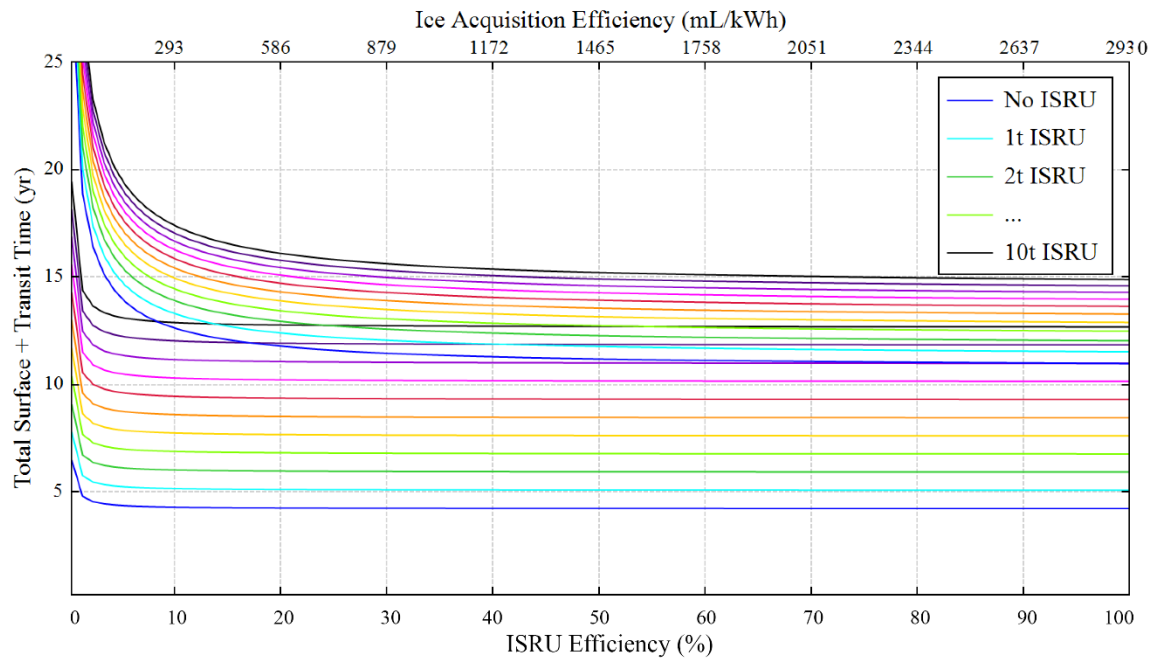
Figure 44: Ideal Mission Times using H₂ from H₂O

Figure 44 shows the relationship between NEP and NTP missions with destinations rich in water-ice. Note the difference in scale for Figure 45 compared to Figure 43, as even at the maximum efficiency, all but the heaviest ISRU systems favor NEP. Here the relatively low hydrogen content of water ice proves far more detrimental to the NTP approach, which must already collect a substantially larger quantity of hydrogen for equivalent performance.
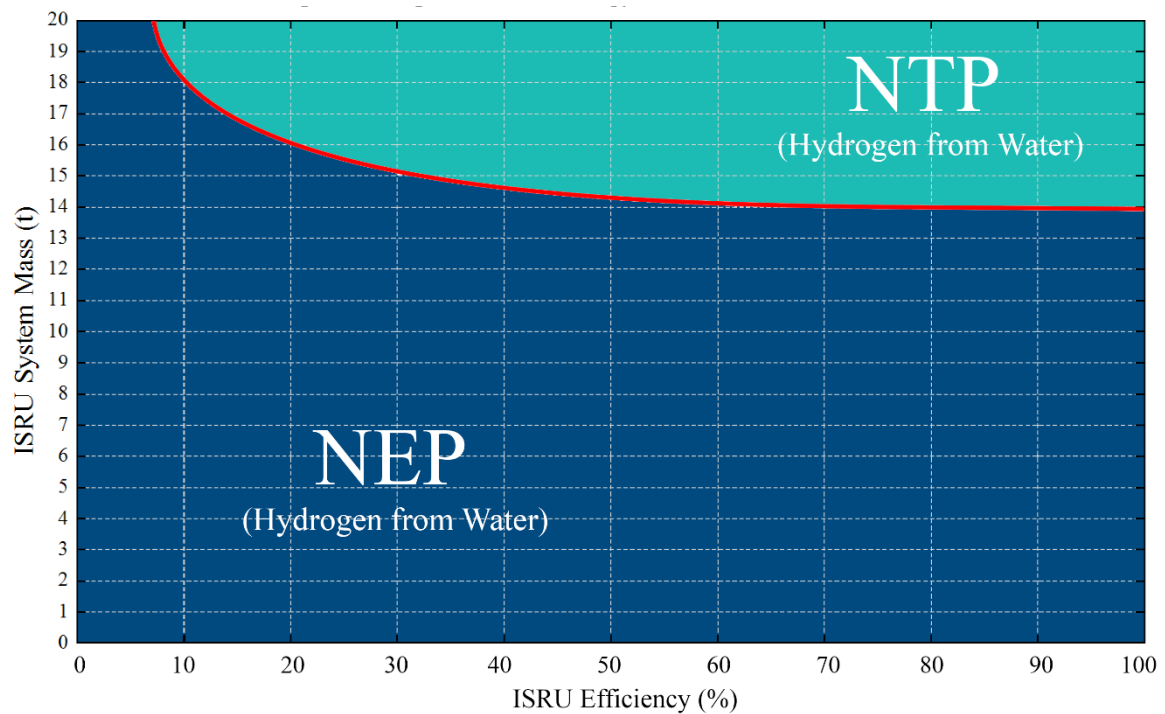
Figure 45: Ideal Propulsion using H₂ from H₂O

39

3.7.3   Methane-Rich Destinations
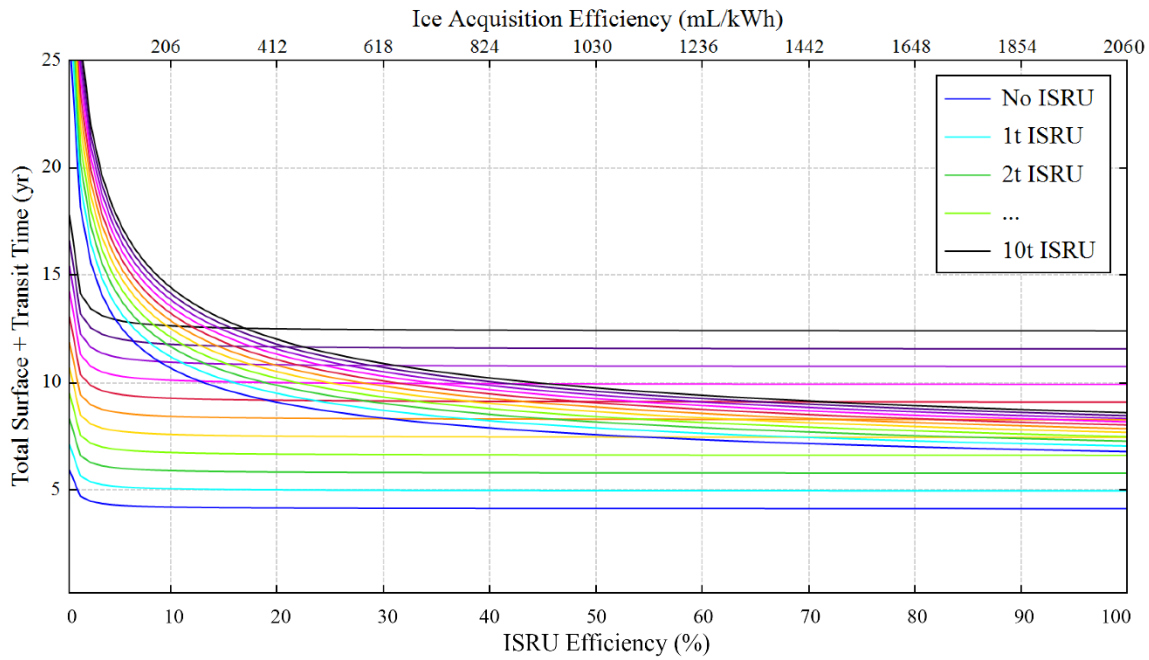
Figure 46: Ideal Mission Times using H₂ from CH₄

Figures 46 and 47 show the mission time comparison for both propulsion systems using hydrogen extracted from methane, while Figures 48 and 49 show the relationship for raw methane. In all cases, despite equal mission time, these comparisons involve substantially different propellant masses be collected, which will be calculated in detail in Section 3.9.
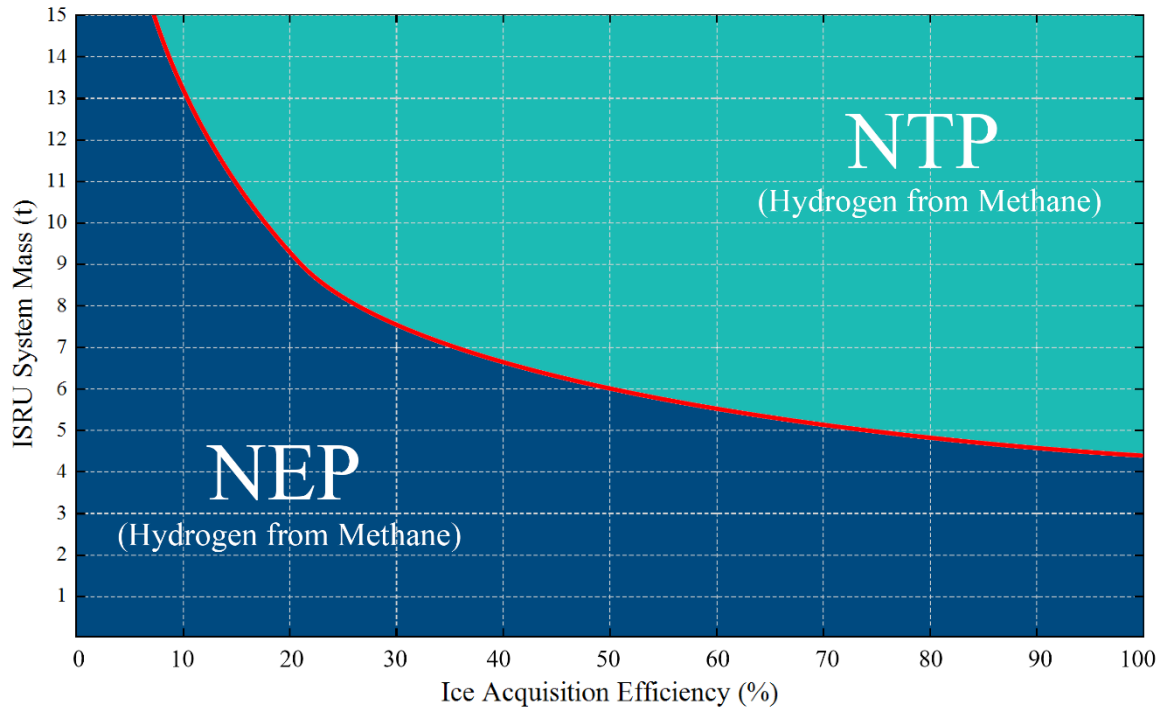
Figure 47: Ideal Propulsion using H₂ from CH₄

NEP	3130	6260	9390	12520	15650	18780	21910	25040	28170	31300
NTP	206	412	618	824	1030	1236	1442	1648	1854	2060
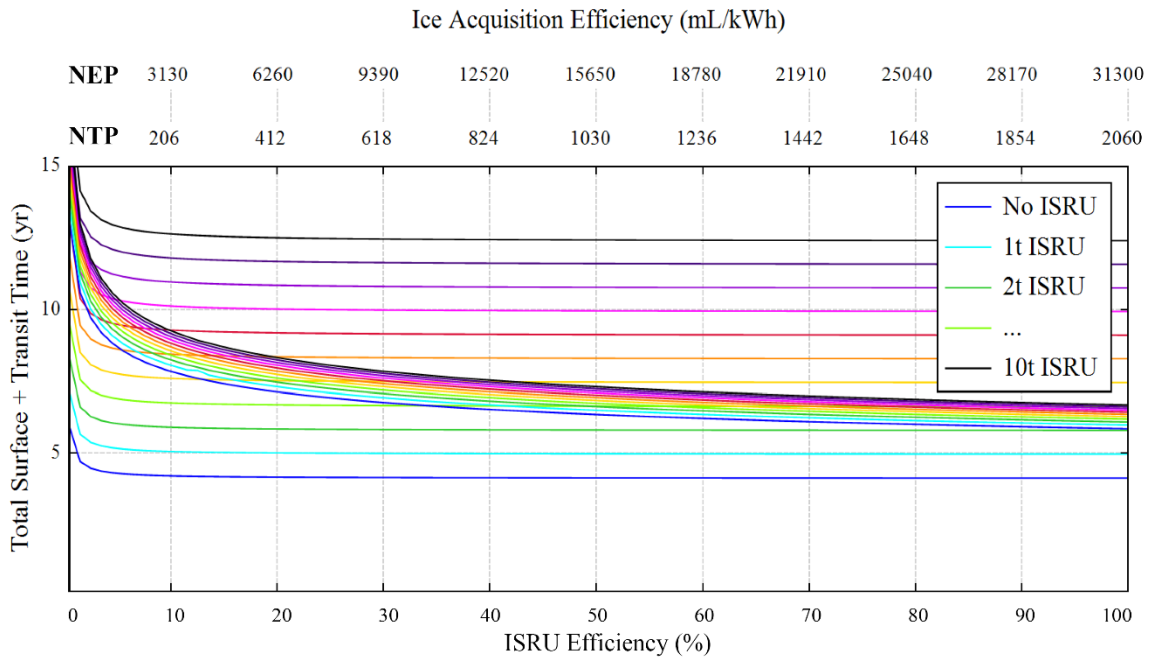
Figure 48: Ideal Mission Times for NEP using H$_2$ from CH$_4$ and NTP using Raw CH$_4$

For all previous cases the acquisition rate has been equal for NEP and NTP. The final scenario features different collection regimes, so the relationship of efficiency to ideal collection rate for each technology is noted at the top of Figure 48. The final relationship in Figure 49 indicates that at such high efficiencies, NTP missions that can utilize raw propellant material have a significant advantage over NEP systems that can only leverage 11.2% of the surface ice collected (which is the weight percentage of the hydrogen within).
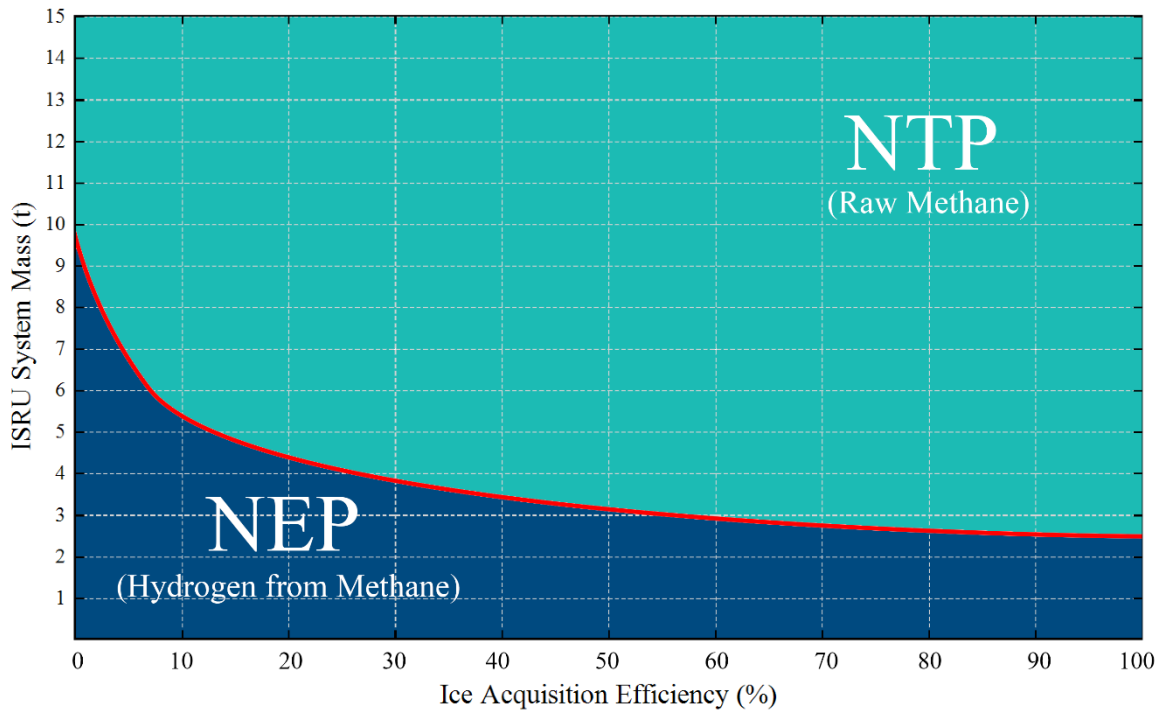
Figure 49: Ideal Propulsion for NEP using H$_2$ from CH$_4$ and NTP using Raw CH$_4$

41

3.8   Leaving the ISRU behind

For the return journey there can be significant savings to jettisoning the ISRU module. The opportunity to push away from this "lower stage" may also help to escape any launch difficulties with KBO gravity. This can be seen in Figure 15 where the module was abandoned but the masses of the larger tanks are still barely noticeable, however there are additional benefits to the low-thrust maneuvers of NEP, where the equations indicate that transit time improves as the spacecraft mass decreases. Figures 50 and 51 show the impact of abandoning the ISRU, where the device is left behind in Figure 51.
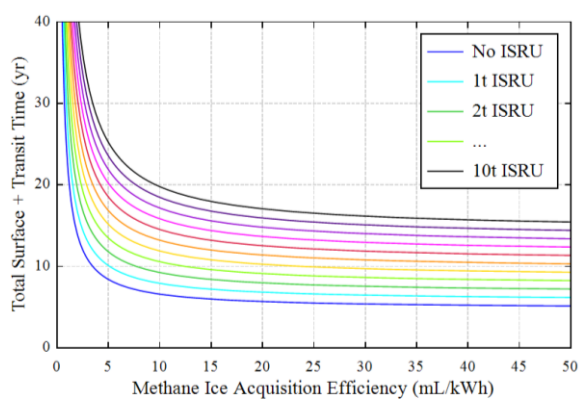
Figure 50: NEP Retaining the ISRU Module   Figure 51: NEP Abandoning the ISRU Module
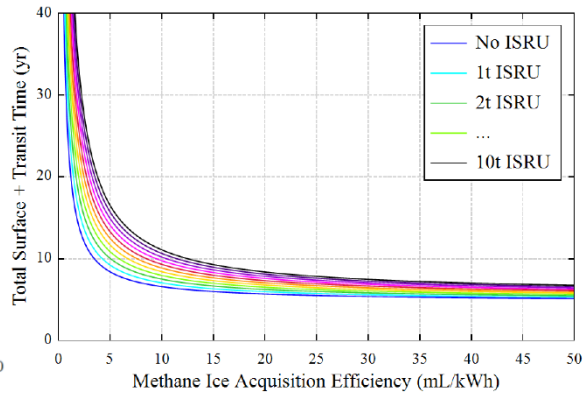
This difference follows the same form for each scenario, and in every case, the impact of the propellant tanks is so small that the contours for abandoned ISRUs collapse towards the relationship given for a weightless ISRU. The NTP system exhibits a similar behavior, as shown in figure 52 and 53. Both the NEP and NTP comparisons are shown for the scenario using hydrogen produced from methane ice.
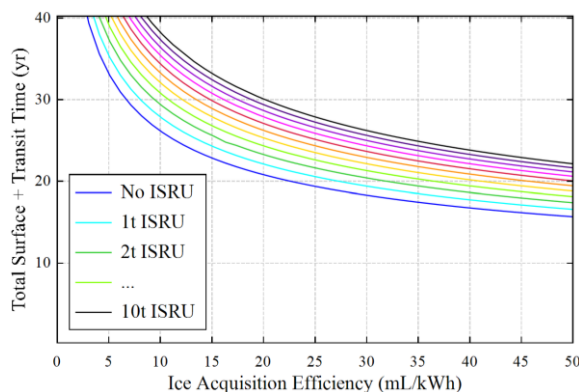
Figure 52: NTP Retaining the ISRU Module   Figure 53: NTP Abandoning the ISRU Module
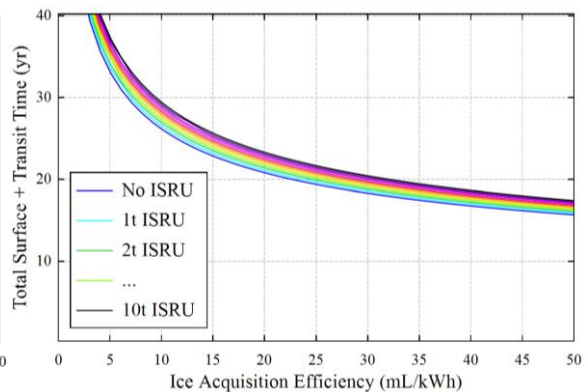
Compared to the previous section, there is no longer a crossover between the technologies within, and plots like Figure 43 would show NEP as the optimal choice at all points.

3.9   Ideal ISRU Parameters

3.9.1   ISRU Efficiency

This ideal definition of efficiency offers a unified impact on mission requirements, however due to the large differences between the energy requirements of each propellant, 50% efficiency may describe a significantly different system for water acquisition compared to nitrogen collection. Below 15% efficiency, the mission times for each propulsion device increase rapidly and diverge from one another for most systems and destinations examined.

3.9.2   System Mass

As shown in plots like Figures 47, the IRSU mass has a variable impact on mission parameters alongside the system efficiency, however a large ISRU can be left behind, whereas a low efficiency system will lengthen the mission regardless of the ISRU mass. There is no ideal tradeoff between system efficiency and system mass for either system, and NTP and NEP have different sensitivities to each of these parameters as shown most clearly in Figure 41. NEP systems perform poorly with heavy ISRU systems due to the physics of spiral maneuvers, while NTP systems can still yield overall superior performance if a heavier ISRU is efficient enough.

3.9.3   Maximum Processing Rate

While the efficiency value is derived from the volumetric energy investment for each propellant material, the power system of the spacecraft is assumed constant at 100kWe. Therefore, the maximum processing rate is unique for each material as shown by Table 9. This value is analogous to the rate at which propellant enters the main storage tank at steady-state and has a perfectly linear relationship with the ISRU efficiency.

Table 9: Maximum Ideal Propellant Collection Rate for each Scenario

Scenario	H2 from CH4	H2 from H2O	CH4	N2
Max Processing Rate (t/hr) (@ 100% efficiency)	0.027	0.031	1.64	3.07

3.9.4 Ultimate Production Capacity

Based on the constant ΔV necessary for NEP's spiral maneuver, the masses of optimal propellant vary with the ISRU mass and system efficiency, shown in Figures 54 and 55. NTP varies based on collection efficiency as well, and Figure 56 displays the ultimate production capacity necessary to achieve optimal ΔV for each propellant at a fixed rate of 100 mL/kWh, which corresponds to the efficiencies listed in Table 10.
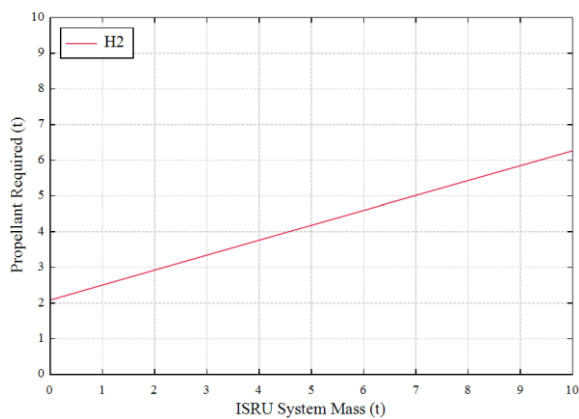
Figure 54: Hydrogen Mass for NEP Spiral
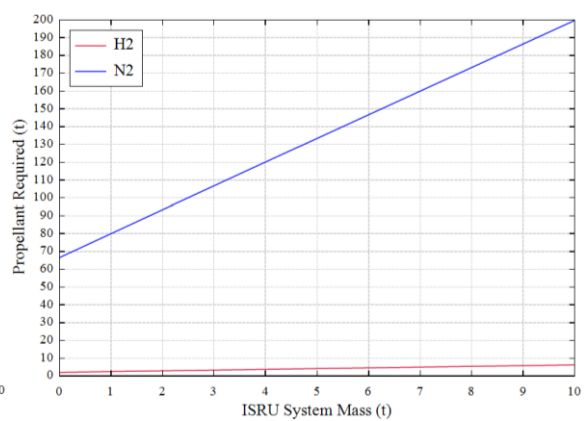
Figure 55: Nitrogen Mass for NEP spiral
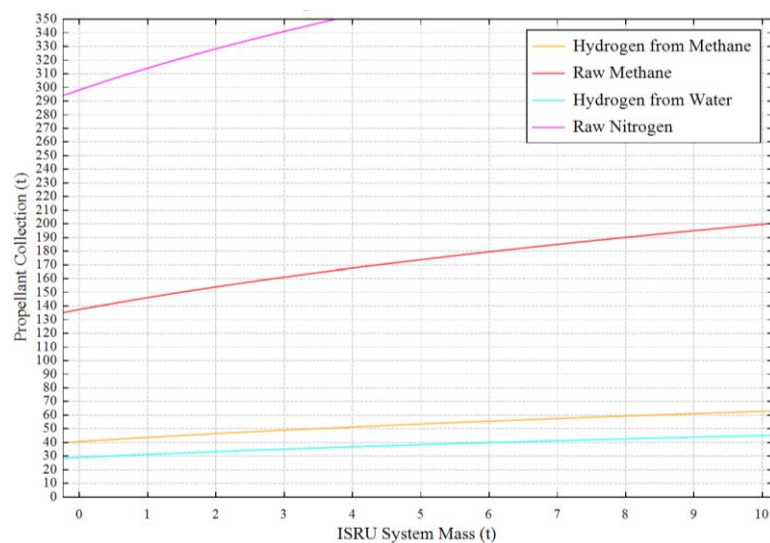
Figure 56: NTP Desired Propellant Mass for a 100 mL/kWh ISRU

Table 10: Equivalent Thermal Efficiency for each Scenario when Operating at 100 mL/kWh

Scenario	H2 from CH4	H2 from H2O	CH4	N2
ISRU Efficiency at 100 mL/kWh	4.8%	3.4%	0.32%	0.13%

3.10 Realistic ISRU Performance for NTP

As shown previously, the propellant acquisition requirements of NEP are smaller, and more constant relative to the quantities preferred by the NTP missions. So far, the wide range of efficiencies examined for ISRU correspond to extremely large quantities for the desired propellant mass. (These are much greater than the original propellant capacity of the spacecraft.) In section 3.6, Figures 26 through 29 indicate that efficiency values as low as 25 to 50 mL/kWh result in a balance at which the optimal ΔV collection equals the original propellant capacity of the spacecraft. Figure 25 compares the effective ΔV of a full tank of each propellant, the mass and performance of which is recorded in Table 11. The tank size examined is for a weightless ISRU for reference, but the equivalent ΔV and transit time are independent of ISRU mass. An example of this analysis is shown between Figures 57 and 58, and the combined results for each propellant are shown in Figure 60.

Table 11: Transit Times and Propellant Masses for the Same Propellant Tank

Scenario	Propellant Mass in Smallest Full Tank (t)	Corresponding ΔV (km/s)	Transit Time (yr)
H2 from CH4	16.2	22.5	15.1
H2 from H2O	16.2	22.5	15.1
Raw CH4	96.4	27.4	12.4
Raw N2	184.2	16.3	18.9
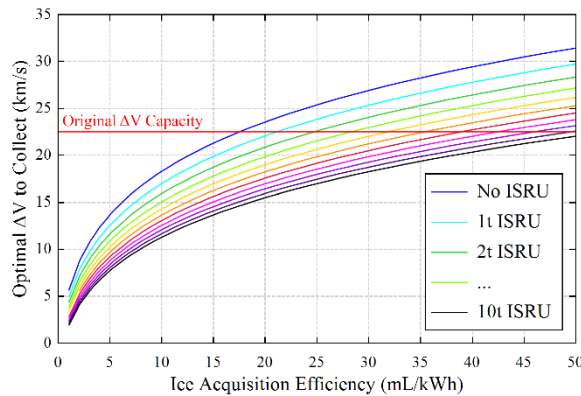
Figure 57: Optimal ΔV for Realistic Capacity   Figure 58: Best ISRU for realistic NTP
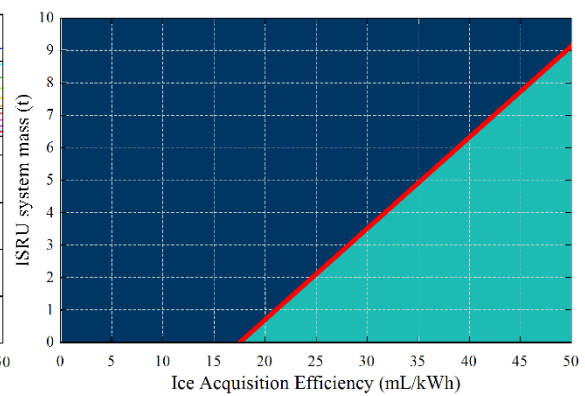
Figure 58 shows two zones, Systems that fall within the dark blue region achieve best mission time while leaving the original propellant tanks only partially filled, while the systems that fall into the lighter region require oversized tanks to leverage the full performance of the ISRU system. Systems described by the red line takes full advantage of the original propellant tanks. This optimal line varies based on the collection scenario.

3.11   Efficiency and Processing

While the value of dissociation for methane only considers the first mole of hydrogen produced, the processing rates assume that 100% of the hydrogen could eventually be extracted from the methane ice. The realistic ISRU efficiencies discussed in the previous section are low enough that energy-based processing requirements are almost negligible but failing to extract all available hydrogen at low collection efficiency can have a large impact on overall system performance. This inaccuracy is partially alleviated by the tendency of dissociated methane to create C-C bonds that make further hydrogen dissociation easier and consolidate the leftover carbon into heavy hydrocarbon waste. (although some hydrogen will always be wasted with it). If significantly less than 2 moles of H_2 can be procured per mole of CH_4, then the results for hydrogen-borne-methane would instead fall within the zone shown in Figure 59.
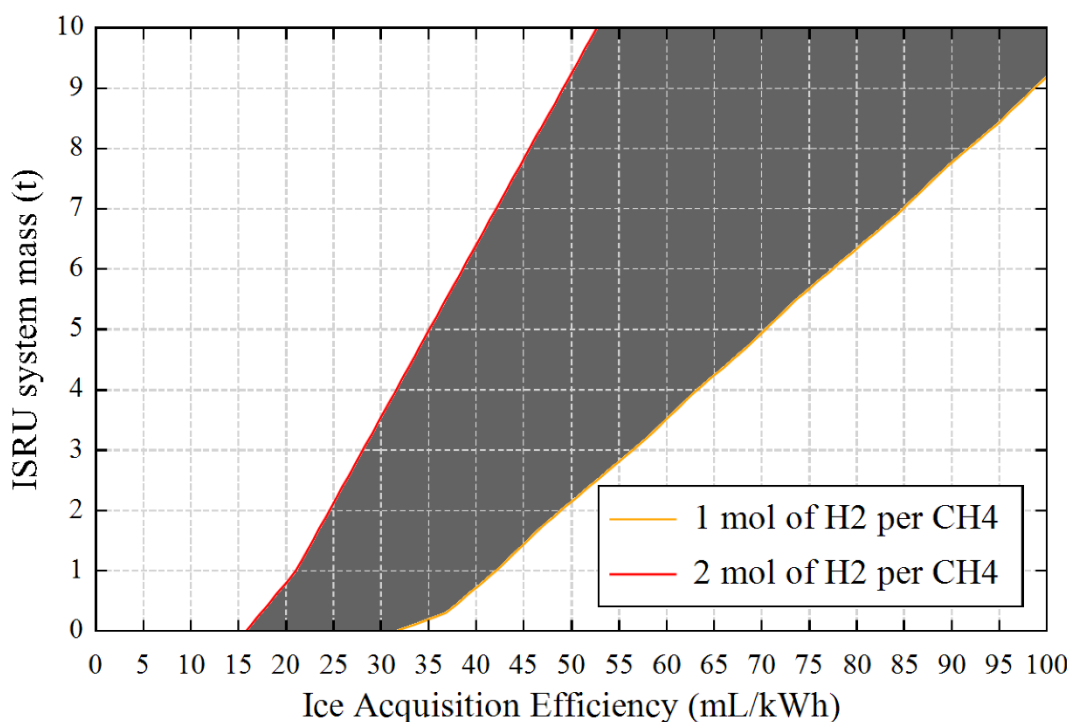
Figure 59: Potential Range of Methane Performance based on Pyrolysis Efficiency

The analysis for water electrolysis also assumes that the vast majority of water collected can be fully decomposed without significant waste of highly ionized water. In addition to high efficiency, both water and methane processing assume that the additional products (carbon and oxygen) will be discarded during processing, while the scenarios for raw propellants assume perfect filtration where necessary.

46

3.12   Final ISRU Parameters for each Scenario using NTP

Figure 60 compares the optimal ISRU system parameters for each collection scenario, and while these relationships are only exact for this example spacecraft, the relative relationship between the scenarios helps to illustrate the larger overall trend for ISRU systems that face such a choice of propellants and destinations. In all cases, the ΔV corresponding to a full propellant tank is assumed to be constant for each scenario, as shown in Figure 24 in Section 3.6. Despite the significantly higher densities of raw methane and nitrogen compared to hydrogen, the surface ice efficiency in terms of volume must still be significantly higher to supply masses of propellant on the order of 100 tonnes.
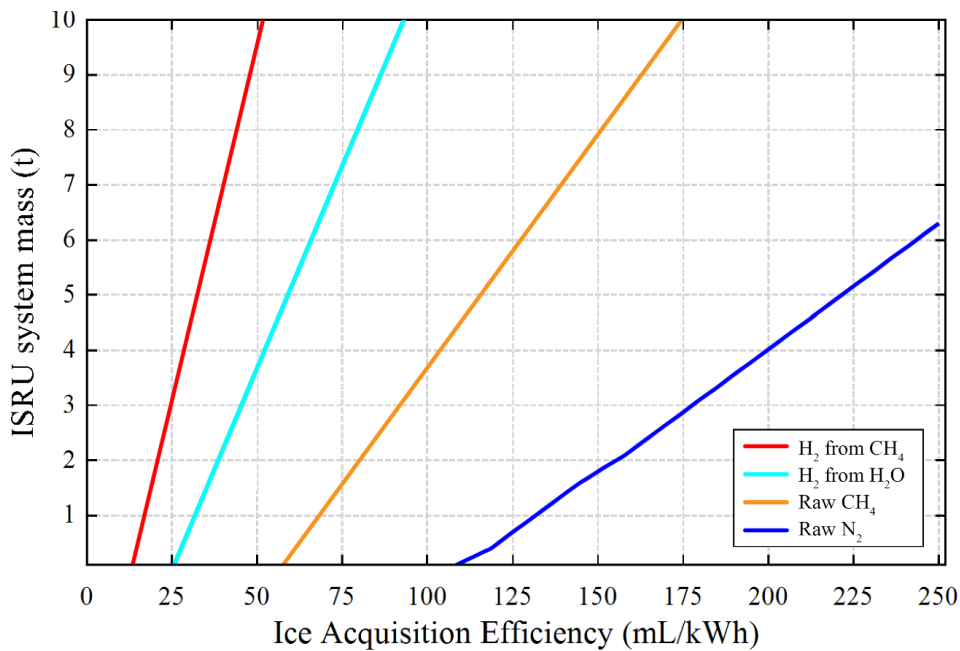
Figure 60: Optimal Parameters of ISRU systems for NTP Missions

Based on these results, if the NTP spacecraft possessed a 4t ISRU, which could collect surface ice at a rate of 75mL/kWh, then without any other adjustments, the tanks would not be sufficient to store the optimal masses of hydrogen, while relying on methane or nitrogen would result in a partially filled tank at departure. Indeed, while Hydrogen is slower to collect and more efficient to use, its low density has a more pronounced impact on these relationships than its high performance compared to the other materials. These ranges indicate that for any realistic propellant acquisition operation, the necessary energy efficiency is so low that the thermal energy investment is practically insignificant by comparison. Therefore, the differences in collection requirements between surface ices are negligible in the range that corresponds to a realistic propellant capacity.

Chapter 4

Conclusion and Future Work

4.1   General Trends

For the NTP system, the most competitive performance is seen when the ISRU system cannot be left behind. Due in part to the nature of impulsive burns, the ideal case for an NTP mission using ISRU therefore involves a large spacecraft with a mission structure that features multiple destinations and thus several opportunities for propellant acquisition. Such a mission would break up the long coasting times where NEP systems offer superior performance. For NEP however, the alternative propellant requirements are so low that for a single destination ISRU appears to be unnecessary for even the most remote locations in the solar system. In addition to the mass tradeoff, problems like the research and development of an ISRU, as well as the time required to collect the necessary departure ΔV are both sidestepped when opting to bring additional propellant from earth.

In-situ propellant acquisition for nuclear propulsion presents significantly more potential benefit to impulsive NTP systems than to NEP. Missions involving a single destination far from the sun play much more to the strengths of NEP, which can realistically accomplish such missions in a similar time without the need of an ISRU system. That said, nuclear systems tend to optimize towards larger missions with multiple destinations, to maximize the benefits that a nuclear reactor can provide and minimize the mass of propellant at each stage of the mission. Based on this analysis, the future applications of ISRU and NTP technology are best suited to the industrialization and commerce of the inner solar system, while NEP systems will offer superior performance to outer solar system destinations of scientific interest (without the need to bring along mining and processing equipment).

4.2 Alternate Mission Requirements

For NEP, the return spiral requires a constant, yet considerable amount of ΔV. By contrast, the NTP system accommodates a variable amount of ΔV, but requires some minimum value to affect a sufficiently linear course, given its dynamic relationship with return time. For comparison, Table 12 shows several missions without ISRU. Several values have been copied from Table 7 as well as Figures 12 to 15. For the case of NTP's optimal return ΔV, the optimal ΔV in the previous scenarios approaches the original propellant capacity of the spacecraft. For this comparison, achieving an equal mission time with the NEP platform would require unrealistic propellant masses (>100t), so this optimal offers a good comparison of a timely return, but still demands an extremely high propellant mass.

Table 12: Required Propellant Mass for Return Journey without ISRU

Platform	Original Propellant Mass (t)	Original wet mass (t)	Original ΔV (km/s)	Return ΔV (km/s)	Additional Propellant (t)	Return time (yr)
NEP	5.37	10.85	53.4	25.23	**5.49**	5.1
NTP (min)	16.2	22.4	22.5	3.58	**4.98**	51.4
NTP (optimal)	ii	ii	ii	22.5	**73.1**	15.1

Table 13 and 14 shows values for theoretical NTP and NEP missions using an ISRU. This system is assumed to be 5 tons and operate at an efficiency of 25 mL/kWh, which results in an initial spacecraft mass of 45 tons, following the trend in Figure 15. these parameters serve to illustrate the center of the realistic ranges examined thus far and ensure that the optimal propellant collection does not exceed the initial tank size for any scenario.

Table 13: Optimal NTP Performance for each Scenario with a fixed ISRU (5t @ 25mL/kWh)

Platform (Scenario)	Surface Ice Processed (t)	Propellant Collected (t)	Optimal Return ΔV (km/s)	Surface and Return time (yr)
NTP (Raw Nitrogen)	138.1	138.1	11.8	24.2
NTP (H_2 from CH_4)	93.6	23.4	19.9	16.2
NTP (H_2 from H_2O)	172.8	19.4	17.5	17.9
NTP (Raw Methane)	71.0	71.0	18.5	17.2

Table 14: Optimal NEP Performance for each Scenario with a fixed ISRU (5t @ 25mL/kWh)

Platform (Scenario)	Surface Ice Processed (t)	Propellant Collected (t)	Required Return ΔV (km/s)	Surface and Return Time (yr)
NEP (Raw Nitrogen)	133.4	133.4	25.23	11.44
NEP (H_2 from CH_4)	16.72	4.18	25.23	6.62
NEP (H_2 from H_2O)	37.32	4.18	25.23	7.17

Comparing the entries for nitrogen in Tables 13 and 14 is especially interesting, because despite expecting a large difference ΔV and transit time, the mass of nitrogen necessary to accomplish this task is the same. For both systems, the mass of nitrogen is an outlier, due to its relatively poor performance as a propellant in both engines.

4.3   Considerations for Mixed Propellant

While this analysis assumed pure surface ice, realistic surface compositions are likely to contain trace amounts of various volatiles as well as regolith and other impurities. In some cases, chemicals like methane and nitrogen may be well mixed, which poses additional challenges to the ISRU. NEP thrusters operate best with a pure monoatomic propellant[35], such that a single ionization is enough to subject a particle to significant force. Ionizing pure nitrogen results in a decrease of MPD efficiency from 50 to 10% compared to pure hydrogen or xenon, so mixing in complex molecules like Water or Methane is likely to be even more detrimental. For NTP systems (which are more compatible with mixed propellants), heavier and more complex molecules will always result in a lower overall I_{sp} and widen the range of potential chemical concerns. It can be shown that the performance of systems like the CNTR is sufficient for volatiles like methane to pack a higher ΔV into the same propellant tank compared pure hydrogen, however a full tank of nitrogen is both heavier and less effective (see Table 11). Mixed propellants hold reasonable potential for NTP if the right combination can be found, but for most materials in the outer solar system chemical incompatibility and low performance make the option unattractive. More ideal combinations of mixed propellants will be discussed in the considerations for future work.

4.4   CNTR Design

So far, the CNTR must already overcome numerous engineering challenges before a prototype can be built, but this technology has the potential to quickly accomplish large and even crewed missions to destinations of unprecedented distance. Traditional SNTP is sufficient for lunar and Martian missions, but the capabilities of the CNTR aim beyond those objectives, which is why this emphasis on additional propellants and destinations is so critical to current design efforts. Based on the findings of this study, while some chemicals like nitrogen make for exceptionally poor propellants (and thus may prevent exploration to some destinations), compatibility with other natural volatiles like methane may lead to significant opportunities for mission architecture and exploration more so than relying on energy intensive processing for hydrogen generation. While the foreseeable scope of nuclear propulsion technology is still limited to the scale of the solar system, a highly versatile and propellant-compatible engine can ideally present a more sustainable and effective approach to space travel, with tangible and achievable benefits in the near term.

4.5   Applications for ideal ISRU

While this analysis primarily examined the benefits of bringing an ISRU module along with a spacecraft to unexplored locations for its own benefit, an ideal ISRU system seems more effective as a stationary depot. While the probes described in this analysis attempt to return to Earth all on their own, such spacecraft could instead be the first phase of a larger mission – designed only to deliver the ISRU. Rather than returning under their own power, these probes could remain on the surface of an important destination and passively collect propellant to resupply a future journey. This approach could enable journeys for small, crewed missions to arrive and depart much more quickly, and this analysis may serve to expand the potential destinations for such preparation. Such depots could also take advantage of their abundant power and propellant to facilitate launch and reentry activities themselves. By seeding key locations in the solar system with autonomous nuclear-powered propellant depots, this technique could eventually form a network of waystations to service far-ranging nuclear-powered spacecraft and enable a wider range of crewed missions.

4.6 Recommended Future Work

At present, nuclear propulsion is still a theoretical approach to future high-performance missions, and significant progress must be made in terms of mission and system design for ISRU to be successfully used in conjunction with the propulsion technologies examined in this analysis. Key research opportunities identified by the author are:

- **Mission Design:** A survey of possible missions with high ISRU-compatibility, which involve multiple destinations of material utility and scientific interest. The best opportunities for such a mission may exist in a 'whistle-stop' exploration of a gas giant's moons, due to their close orbits and accessible surface ice.

- **CNTR Operation:** The parameters for reactor operations in a passive solid-state mode, as well as the energy requirements to sustain a molten core for extended periods of time, to determine and improve the capacity for electricity generation.

- **ISRU Systems:** The conceptual design of efficient mining systems or passive propellant collection techniques to determine the expected performance and special considerations for ISRU-based missions to each potential destination.

- **NTP Propellants:** Material interactions with alternate propellants at NTP temperatures, including long-term exposure and mixed propellant testing. For the CNTR in particular, direct contact between propellant material and nuclear fuel presents a wider range of potential interactions to investigate. Also, future ISRU missions may benefit from knowing the exact performance of mixed propellants that correspond to the surface composition of the destination. In the Kuiper belt, the potential mixtures listed in Table 1 offer reduced performance compared to pure propellants, but if a target body ever presents lighter materials with methane-like performance such as ammonia[3] and lithium hydride salts,[40] then mixed in-situ propellants may be a reasonable strategy for those NTP-based missions.

Ultimately, the potential applications of ISRU and Nuclear propulsion technologies extend well beyond the current era of space exploration and represent the larger paradigm shift from conflict to collaboration with the natural environment. Therefore, these technologies also depend on deeper exploration of the solar system to uncover more about the material nature of the space environment and extend future missions to the edge of possibility.

Bibliography

1. Finseth JL. *Rover Nuclear Rocket Engine Program: Overview of Rover Engine Tests*.; 1991. Accessed April 25, 2023. https://ntrs.nasa.gov/citations/19920005899

2. Borowski S, Dudzinski L, McGuire M. Vehicle and mission design options for the human exploration of Mars/Phobos using "bimodal" NTR and LANTR propulsion. In: *34th AIAA/ASME/SAE/ASEE Joint Propulsion Conference and Exhibit*. American Institute of Aeronautics and Astronautics; 1998. doi:10.2514/6.1998-3883

3. Nikitaev D, In-Situ Alternative Propellants for Nuclear Thermal Propulsion. AIAA Propulsion and Energy Forum. doi:10.2514/6.2021-3597

4. Heidet F, Foster J, Patterson M, et al. Overview of High-Performance Centrifugal Nuclear Thermal Rocket Propulsion System. In: *Transactions of the American Nuclear Society - Volume 123*. AMNS; 2020:42-46. doi:10.13182/T123-33578

5. Choueiri EY, Ziemer JK. Quasi-Steady Magnetoplasmadynamic Thruster Performance Database. *J Propuls Power*. 2001;17(5):967-976. doi:10.2514/2.5857

6. Gilland J, Myers R, Patterson M. Multimegawatt electric propulsion system design considerations. Published online September 1, 1991. doi:10.2514/6.1990-2552

7. McGuire ML. High Power MPD Nuclear Electric Propulsion (NEP) for Artificial Gravity HOPE Missions to Callisto. In: *AIP Conference Proceedings*. Vol 654. AIP; 2003:837-843. doi:10.1063/1.1541375

8. Landis GA, Oleson SR, Abel P, et al. Missions to Triton and Pluto using a Hopper Vehicle with In-Situ Refueling. In: ; 2019. Accessed April 26, 2023. https://ntrs.nasa.gov/citations/20190032656

9. Chato D. Refueling with In-Situ Produced Propellants. Presented at: 20 th Advanced Space Propulsion Workshop; November 18, 2014. https://ntrs.nasa.gov/api/citations/20150002711/downloads/20150002711.pdf

10. Stern SA, Bagenal F, Ennico K, et al. The Pluto system: Initial results from its exploration by New Horizons. *Science*. 2015;350(6258):aad1815. doi:10.1126/science.aad1815

11. Brown ME. The Compositions of Kuiper Belt Objects. *Annu Rev Earth Planet Sci*. 2012;40:467-494. doi:10.1146/annurev-earth-042711-105352

12. Owen TC, Roush TL, Cruikshank DP, et al. Surface Ices and the Atmospheric Composition of Pluto. *Science*. 1993;261(5122):745-748. doi:10.1126/science.261.5122.745

13. Dumas C, Merlin F, Barucci MA, et al. Surface composition of the largest dwarf planet 136199 Eris (2003 UB$\{_{313}\}$). *Astron Astrophys*. 2007;471(1):331-334. doi:10.1051/0004-6361:20066665

14. Haumea | Ring, Moons, Composition, & Name | Britannica. Accessed April 26, 2023. https://www.britannica.com/place/Haumea

15. Trujillo CA, Brown ME, Rabinowitz DL, Geballe TR. Near-Infrared Surface Properties of the Two Intrinsically Brightest Minor Planets: (90377) Sedna and (90482) Orcus*. *Astrophys J*. 2005;627(2):1057. doi:10.1086/430337

16. Barucci MA, Dalle Ore CM, Perna D, et al. (50000) Quaoar: Surface composition variability. *Astron Astrophys*. 2015;584:A107. doi:10.1051/0004-6361/201526119

17. Rumble JR, ed. *CRC Handbook of Chemistry and Physics*. 102nd edition 2021-2022. CRC Press; 2021.

18. Sánchez-Bastardo N, Schlögl R, Ruland H. Methane Pyrolysis for Zero-Emission Hydrogen Production: A Potential Bridge Technology from Fossil Fuels to a Renewable and Sustainable Hydrogen Economy. *Ind Eng Chem Res*. 2021;60(32):11855-11881. doi:10.1021/acs.iecr.1c01679

19. Sagmiller D, Hartwig J. Survey of Cryogenic Nitrogen Thermomechanical Property Data Relevant to Outer Solar System Bodies. *Earth Space Sci*. 2020;7(9):e2019EA000640. doi:10.1029/2019EA000640

20. Properties of Various Ideal Gases (at 300 K). Accessed April 25, 2023. https://www.ohio.edu/mechanical/thermo/property_tables/gas/idealGas.html

21. Hendrie JM. Dissociation Energy of N2. *J Chem Phys*. 2004;22(9):1503-1507. doi:10.1063/1.1740449

22. Ziehm W, Thomas L. Correction: Mission Design Analysis with Centrifugal Nuclear Thermal Propulsion. In: *AIAA SCITECH 2023 Forum*. AIAA SciTech Forum. American Institute of Aeronautics and Astronautics; 2023. doi:10.2514/6.2023-0153.c1

23. Houts MG, Lenard RX, Lipinski RJ, Patton B, Poston DI, Wright SA. *NEP for a Kuiper Belt Object Rendezvous Mission*. Sandia National Lab. (SNL-NM), Albuquerque, NM (United States); Sandia National Lab. (SNL-CA), Livermore, CA (United States); 1999. Accessed April 25, 2023. https://www.osti.gov/biblio/15019

24. Kumar S, Thomas LD, Cassibry JT. Nuclear Thermal Propulsion for Jupiter and Saturn Rendezvous Missions. *J Spacecr Rockets*. Published online February 2, 2022. doi:10.2514/1.A35212

25. Drake BG. Human Exploration of Mars Design Reference Architecture 5.0 Addendum. Published online 2009.

26. Borowski SK, Ryan SW, Burke LM, McCurdy DR, Fittje JE, Joyner CR. Robust Exploration and Commercial Missions to the Moon Using LANTR Propulsion and In-Situ Propellants Derived from Lunar Polar Ice (LPI) Deposits. In: *AIAA SPACE and Astronautics Forum and Exposition*. American Institute of Aeronautics and Astronautics. doi:10.2514/6.2017-5272

27. Nuclear Thermal Propulsion Engine Minimally-Intrusive Power Generation Alternatives. AIAA Propulsion and Energy Forum. doi:10.2514/6.2021-3605

28. Litchford RJ, Harada N. Multi-MW Closed Cycle MHD Nuclear Space Power Via Nonequilibrium He/Xe Working Plasma. Published online 2011.

29. Houts M, Thomas LD, Nassersharif B. CENTRIFUGAL NUCLEAR THERMAL ROCKET CHALLENGES AND POTENTIAL. doi:AAS 23-175

30. Vardaxis G, Pitz A, Wie B. AAS 12-128 CONCEPTUAL DESIGN AND ANALYSIS OF PLANETARY DEFENSE TECHNOLOGY (PDT) DEMONSTRATION MISSIONS. Published online April 26, 2023.

31. Tsuda Y, Yoshikawa M, Abe M, Minamino H, Nakazawa S. System design of the Hayabusa 2—Asteroid sample return mission to 1999 JU3. *Acta Astronaut*. 2013;91:356-362. doi:10.1016/j.actaastro.2013.06.028

32. Sovey J, Mantenieks M. Performance and lifetime assessment of MPD arc thruster technology. In: *24th Joint Propulsion Conference*. American Institute of Aeronautics and Astronautics; 1988. doi:10.2514/6.1988-3211

33. Mcgranaghan R, Sagan B, Dove G, Tullos A, Lyne J, Emery J. A Survey of Mission Opportunities to Trans-Neptunian Objects. *J Br Interplanet Soc*. 2011;142:296-303.

34. Brown ME. The Largest Kuiper Belt Objects.

35. Jhan RG. *Physics of Electric Propulsion*. McGRAW-HILL; 1968.

36. Pietrobon SS. Analysis of Propellant Tank Masses.

37. Small-Body Database Lookup. Accessed April 26, 2023. https://ssd.jpl.nasa.gov/tools/sbdb_lookup.html#/

38. Gaylor D. *LOW THRUST CIRCLE-TO-CIRCLE ORBIT TRANSFER*.; 2002.

39. Prussing JE, Conway BA. *Orbital Mechanics*. Second edition. Oxford University Press; 2013.

40. Krieger FJ. *A Parametric Study of Certain Low-Molecular-Weight Compounds as Nuclear Rocket Propellants-IV: Lithium Hydride*. RAND Corporation; 1959. Accessed April 26, 2023. https://www.rand.org/pubs/research_memoranda/RM2403.html

Appendix A

(Concurrent research relevant to material processing with nuclear technology)

Conceptual Study of Hydrogen Generation with Cobalt-60 Through Radiolysis

Introduction

Hydrogen production is projected to increase as the world moves toward carbon-free energy sources. Even in a nuclear power plant (NPP), about 74 kW of equivalent hydrogen is used for coolant chemistry control to support daily operation. At present, carbon-free hydrogen can be produced by devoting renewable or nuclear energy to systems like electrolysis. Inside an NPP, the intense radiation environment of the core splits the water molecules via radiolysis. Capturing this generated hydrogen is a futile effort due to activation, safety implication, efficiency, and high probability for recombination. On the other hand, through the activation of Cobalt 59 in the NPP core, the intense radiation of a reactor core can be transferred to an external apparatus in order to decompose water molecules into hydrogen and oxygen. The design for this radiation receptacle includes a dense matrix of alumina, in order to promote radiolysis. This summary explores the operation scheme and material requirements of a radiolysis machine that operates within the NPP site boundary to supply hydrogen for on-site and off-site activities.

Concept and Operation

Cobalt-60 (~5-year half-life) decay allows for continuous operation in steady state for long periods. In order to obtain Cobalt-60 while minimizing the disruption to the core and promote reusability, natural cobalt is loaded into an empty fuel assembly, which replaces a bundle on the core periphery. During a refueling outage, this bundle is extracted and transported in cask into a tall cylindrical tank of water as shown in Figure. A-1.
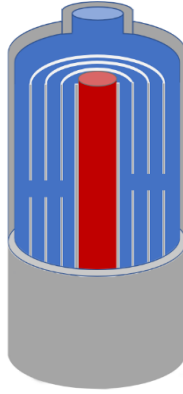
Figure A-1. Receptacle design with photoelectric material layers

For simplicity, the receptacle is cylindrical, with radioactive material at the center. Because Cobalt 60 decays with a single strong gamma emission, thin structures photoelectric material can be optimized to deposit this energy in the water to maximize ionization[1].

Production Targets and Constraints

During normal operation, a nuclear plant devotes about 74kW of electrical energy towards water electrolysis machines, in order to supply on-site hydrogen demand (particularly for primary water chemistry control). While this data was obtained from plant operators, it does not reflect a true average, and so can vary with the location and design of the plant. In general, electrolysis machines in this application require 54 kW per kg of hydrogen produced[2]. Using these numbers, the total production target is calculated below.

$$74 \ kW \ \div \ 54 \frac{kWh}{kg} H_2 \ \rightarrow \ 12{,}012 \frac{kg}{yr} H_2 \qquad (1)$$

Material and Geometry

In order to accommodate the on-site demands of roughly 12,000 kg of Hydrogen per year (as calculated in previous subsection), it is essential to calculate a rough energy-efficiency of radiolysis based on the experimental production rates observed under known energy-depositions. In a study of water decomposition under radiation by Yoshida[1], once photoelectric material was introduced to water under CO-60 gamma radiation, a constant production rate accumulated 6.29E-5 moles of H2 for each mole of H2O present.

In thermodynamically perfect conditions, it takes 237 kJ of energy to dissociate one mole water into component molecules. These free atoms can then recombine as either molecular hydrogen or otherwise form back into larger molecules like water, peroxide, and ozone.

That energy of recombination is released as thermal energy which is assumed not to contribute towards ionization. Using experimental values from the work by Yoshida[1], each mole (~18g) of water present absorbed roughly 82 Joules after one hour of irradiation. By using the production rate observed under these conditions, the following expression yields a value for overall radiolysis efficiency

$$\frac{237\ kJ}{\left(1\frac{mol\ H_2}{mol\ H_2O}\right)} = \eta * \frac{82.2\ J}{\left(6.288*10^{-5}\frac{mol\ H_2}{mol\ H_2O}\right)} \rightarrow \eta = 18.2\% \tag{2}$$

This efficiency is significantly lower than PEM electrolysis, which is roughly 40% energy efficient. This factor enables calculating the amount of radioactive material needed, as the total energy of ionizing radiation must provide at least:

$$\left(\frac{237\ kiloJoule}{1\ mol\ H_2}\right) \times \eta \div 2\frac{g}{mol}\ H_2 * 12{,}012\frac{kg}{yr} = 248\ kW \tag{3}$$

Based on experimental data by Yoshida, this power is the minimum necessary to ensure the hydrogen production rate accommodates demand at all times. Based on the decay rate of Cobalt-60, the average decay energy, and the energy of each emission, the required mass of radioactive material necessary to provide this power would be:

$$\frac{248\ kW}{\gamma_{Co^{60}}} = 3.22\ Ci \rightarrow \frac{3.22\ Ci}{\lambda_{Co^{60}}} * \frac{60\frac{g}{mol}}{\#_{Avg}} = 28.6\ kg \tag{4}$$

Due to radioactive decay over the operational cycle of the reactor (18 months), this means that the activity and mass of Cobalt-60 freshly extracted from the reactor can be found as:

$$3.22\ Ci = A_0 * e^{-\lambda_{Co^{60}}*(4.7*10^7 s)} \tag{5}$$

$$\frac{A_0}{\lambda_{Co^{60}}} * \frac{60\frac{g}{mol}}{\#_{Avg}} = 35.9\ kg \tag{6}$$

Because activation takes place in the core periphery, Figure 6 from Allen's report on cobalt production at Savannah River[3] can be used to determine that the expected activation of Cobalt-59, approaches 20% for this exposure time. Therefore, the core requires roughly 180 kg of Cobalt-59 in order to generate 18 months' worth of hydrogen. Depending on type of reactor (e.g., PWRs or BWRs), this quantity can fit roughly into one or two fuel assemblies, (these assemblies could take advantage of lost neutrons in the periphery of the core to achieve activation without compromising overall reactivity or burnup). While higher activation would be ideal due to a lower raw material requirement, 2D lattice reactor physics simulations of deep-core cobalt insertions necessary to leverage higher neutron fluxes indicate that cycle economics would be irrecoverably compromised.

As was briefly mentioned previously, the most efficient approach to cobalt activation requires an easily insertable and transportable structure that spans the entire active length of the core. While an empty zircalloy fuel bundle would ultimately be more expensive than the raw cobalt it would be used to contain, using such an assembly would also aid ease of installation, safety, and simplicity for the rest of the surrounding infrastructure.

By using a cobalt source in the form of a 4-meter-long fuel element, the receptacle and its feedstock could be more efficiently shaped into a cylinder along that length, rather than the spherical solution envisioned previously. The Tenth-Value-Layer (TVL) of Co60 gammas in water is 37.5 cm[4]. Therefore, in order to ensure that more than 99% of radiation energy is deposited in the receptacle's feedstock, the cylindrical tank would only need a diameter of 1.5 meters. This means that the receptacle could be built around a single 2000 Gallon steel tank. Cylindrical water tanks of this size are relatively cheap among prefab stainless-steel structures, and the ease of assembly would help to make the installation of alumina significantly more straightforward.

Drawing further on simulations performed in Yoshida 2007, the optimal thicknesses and spacings of photoelectric material were found to be 1 mm and 1 cm respectively. This arrangement can be seen in Figure 2. There is very little performance falloff up to a gap of 2cm, which makes it an excellent choice for cost savings and operation with high flowrate. The surface area of this alumina structure was found from equation 7, for a full-length and nested structure of layers (1mm thick).

$$\sum_{r=10}^{75} 2 * \pi * r * h = 716.28 \ m^2 \tag{7}$$
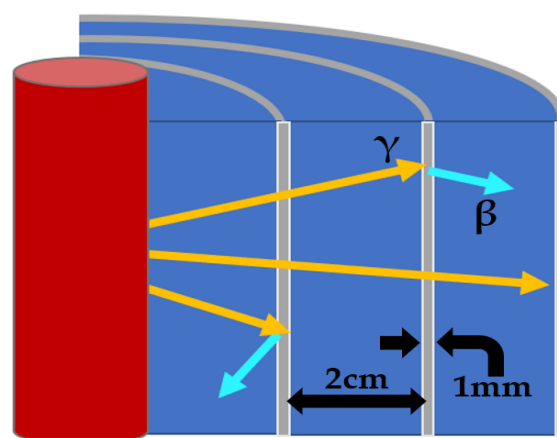

Figure A-2. Geometry and operation of photoelectric material

Enhancements to Operation Scheme

With the radius and internal geometry described, the effectiveness of this design depends on maintaining flow conditions that prevent recombination, as well as the efficient activation of the cobalt source. In the electrolysis of water, the high electrical bias that pulls water molecules apart automatically separates the atomic species and allows their separate extraction; under intense irradiation, the hydrogen and oxygen are instead mixed uniformly in the water and are more prone to recombine than to separate naturally. However, there is a voltage threshold of 0.4V below which electrolysis cannot separate water molecules on its own [5]. If a voltage below this threshold were to be applied along the length of the tank, then a hydrogen/oxygen segregation could significantly hamper the natural recombination rate without a serious investment of electrical power. If the receptacle wall is an anode, while the cathode is radially central. In concert with some gaps in the alumina layers, a small electrical bias may serve as the primary method of gas collection.

While higher G-values appear at higher temperatures, the recombination rate of hydrogen and oxygen ions in water is much more responsive to temperature than any theoretical improvement to water radiolysis. While recombination and ease of dissociation both increase at higher temperatures, the G-value of water is fairly constant until temperatures reach 200 Celsius [6]. By comparison, the recombination rate of hydronium and hydroxide observed in ionized water more-than-doubles in the range between 0 and 50 Celsius [7] because recombination is so deleterious to the overall production rate, it is best to minimize both trends by operating at as low of a temperature as feasible.

While a low activation regime as described (max 20%) requires a large amount of cobalt to make practical, one serious advantage of using large fuel assemblies of cobalt is the opportunity to repeatedly exchange a small number of assemblies between the core and the receptacle over several decades. Due to the long half-life of cobalt 60 and the relatively short cycle length necessary to activate it, two 180kg bundles that repeatedly trade places between activation in the core and decay in the receptacle may continue to reach the necessary 20% activation even after 10 years of operation. In order to accommodate core symmetry, the cobalt may need to be split between two fuel assemblies, even if it occupies a space on the periphery.

Value Proposition

For electrolysis machines, the operating costs of equipment replacement and electrical consumption are of roughly the same order [2]. The overall expense per kilogram of hydrogen produced and the annual cost can be found as:

$$\left(54\frac{kW}{kg} * 11.2\frac{¢}{kWh}\right) + 5\frac{\$}{kg} = 11.05\frac{\$}{kg} \tag{8}$$

$$11.05\frac{\$}{kg} * 12{,}012\frac{kg}{yr} = 132{,}732\frac{\$}{yr} \tag{9}$$

This value offers a conservative estimate using 2021 data, as it will increase proportionally with the cost of electricity. With this value in mind, a radiolysis machine must offer a lower yearly expense in order to recoup the cost of its initial construction and make installation a worthwhile prospect.

By contrast, the two major expenses associated with radiolysis come in the form of raw cobalt, and the lost core burnup necessary for activation. Cobalt prices are prone to large spikes, but the average cost since 2018 has been roughly 75 USD per kg [8]. Using the values found from (6) the total annual cost of cobalt can be found as:

$$\frac{35.9\frac{kg}{cycle}}{20\%\ \text{activation}} * 75\frac{\$}{kg} * \frac{2\ cycles}{3\ yr} = 9{,}874\frac{\$}{yr} \tag{10}$$

Additionally, inserting this raw cobalt into the reactor core for activation introduces a neutron poison that has a small but noticeable effect on core economics. Inserting a cobalt-filled fuel assembly in the periphery of a BWR results in the loss of 1 assembly out of approximately 750. Power in the periphery is typically less than 1/3 of the core average. This noticeably reduces the overall core power by one half of a MW_{th}. This expense was evaluated using the EIA cost for nuclear electricity [9] and a thermal efficiency of 35% [10].

$$\frac{1}{2}MW_{th} * \eta_{th} * 30\frac{\$}{MWh} = 53{,}690\frac{\$}{yr} \tag{11}$$

These values combined yield a lower annual operating cost than the equipment and electricity necessary for electrolysis (Even if two fuel assemblies are necessary to maintain core symmetry). The up-front installation costs of this system will include the roughly 2000-gallon stainless steel water tank, 716 square meters of alumina, and at least one empty zirconium fuel assembly depending on the reactor type. The final costs for an example BWR are presented in Table 1. Assuming factor of 2x cost for labor and installation, the cost of a radiolysis machine can be in-line and competitive with electrolysis.

Table A-1. Radiolysis Capital Investment
Up-front cost by component

Component	Cost Factor	Total
fuel assemblies	300 \$/kg [11]	\$54,000
Cobalt-59 (180 kg)	75 \$/kg [8]	\$9,874
Alumina (2,800 kg*)	†41 \$/kg [13]	\$115,956
Receptacle (2000 gal)	2.5 \$/gal [15]	\$5,000
Capital Cost		**\$184,830**

Conclusion

While reactor cores are too sensitive and complex to effectively generate hydrogen from within primary containment, the designs put forward in this work serves to improve the utilization of radiation energy at a competitive scale and efficiency

In order to fully realize this design, the dynamics of water recombination under ionizing radiation and low voltage must be better defined. Additionally, the gas extraction system and storage would need to be carefully design based on regulatory and safety considerations.

Nomenclature

η = Energy efficiency of radiolysis
H_2 = Molecular hydrogen
Co^{60} = Cobalt 60
$\gamma_{Co^{60}}$ = Gamma decay of Cobalt 60 ($1.25\ MeV$)
$\lambda_{Co^{60}}$ = Decay Constant of Cobalt 60
$\#_{Avg}$ = Avogadro's number
\$ = 2021 United States Dollar

Acknowledgements

---

* Alumina mass calculated with a density of 3.97 g/cm^2 [12]
† Converted to 2021 dollars from 35 \$/kg in 2016 (CPI)[14]

References

1. Yoshida, T., Tanabe, T., Sugie, N., & Chen, A. (2007). Utilization of gamma-ray irradiation for hydrogen production from water. Journal of Radioanalytical and Nuclear Chemistry, 272(3),471–476. https://doi.org/10.1007/s10967-007-0606-2

2. Lichner, C. (2021, April 5). *Electrolyzer Overview: Lowering the cost of hydrogen and distributing its production*. pv magazine USA. Retrieved June 3, 2022

3. Allen, H. F. (1964). Cobalt-60 production at savannah river. Process Radiation Meeting, 12. Retrieved June 4, 2022, from https://www.osti.gov/servlets/purl/10115642.

4. Biswas, R., Sahadath, H., Mollah, A. S., & Huq, M. F. (2016). Calculation of gamma-ray attenuation parameters for locally developed shielding material: Polyboron. Journal of Radiation Research and Applied Sciences, 9(1), 26–34. https://doi.org/10.1016/j.jrras.2015.08.005

5. Tebibel, H., & Medjebour, R. (2018). Comparative performance analysis of a grid connected PV system for hydrogen production using PEM water, methanol and hybrid sulfur electrolysis. International Journal of Hydrogen Energy, 43(6), 3482–3498. https://doi.org/10.1016/j.ijhydene.2017.12.084

6. Elliot, A. J., Chenier, M. P., & Ouellette, D. C. (1990). g-values for γ-irradiated water as a function of temperature. Canadian Journal of Chemistry, 68(5), 712–719. https://doi.org/10.1139/v90-111

7. Natzle, W. C., & Moore, C. B. (1985). Recombination of hydrogen ion (H+) and hydroxide in pure liquid water. The Journal of Physical Chemistry, 89(12), 2605–2612. https://doi.org/10.1021/j100258a035

8. *Cobalt Price*. Dily Metal Price. (n.d.). Retrieved June 2, 2022, from
   https://www.dailymetalprice.com/cobalt.html
   https://www.dailymetalprice.com/metalpricecharts.php?c=co&u=lb&d=0

9. *Annual Energy Outlook - U.S. Energy Information Administration (EIA)*. Annual
   Energy Outlook 2022 - U.S. Energy Information Administration (EIA).
   (2021). Retrieved June 11, 2022, from https://www.eia.gov/outlooks/aeo/

10. Ibrahim, S. M., Ibrahim, M. M., & Attia, S. I. (2014). The impact of climate changes
    on the thermal performance of a proposed pressurized water reactor: Nuclear-
    power plant. *International Journal of Nuclear Energy*, *2014*, 1–7.
    https://doi.org/10.1155/2014/793908

11. *Economics of Nuclear Power*. Nuclear Power Economics | Nuclear Energy Costs -
    World Nuclear Association. (2021, September). Retrieved June 11, 2022,
    from https://world-nuclear.org/information-library/economic-
    aspects/economics-of-nuclear-power.aspx

12. U.S. National Library of Medicine. (2022). *Aluminum oxide*. National Center for
    Biotechnology Information. PubChem Compound Database. Retrieved June
    11, 2022, from https://pubchem.ncbi.nlm.nih.gov/compound/ Aluminum-
    oxide#section=Density

13. Crouch, I. G. (2017). Trends in armor materials. In Science of Armor Materials (p.
    688). essay, Woodhead Publishing.

14. U.S. Bureau of Labor Statistics. (n.d.). *CPI inflation calculator*. Charts and
    Applications. Retrieved June 11, 2022, from
    https://www.bls.gov/data/inflation_calculator .htm

15. Allgrove, R. J. (2020, April 8). Water Storage Tank Assessments - Environmental
    Partners Group, Inc. Foxborough, MA; Department of Public Works.